SHIV-NI (MM428, MM432, and MM434; $n=3$). Monkeys were inoculated intravenously with 10^5 $TCID_{50}$ of each virus. At 8 wpi, all animals were challenged intravenously with a 10^5 $TCID_{50}$ of pathogenic SHIV-C2/1 KS661. Citrate-anticoagulant blood samples were collected under anesthesia with ketamine hydrochloride. Blood samples were phenotypically characterized on a FACSCaliber flow cytometer (Becton Dickinson, San Jose, CA) and were separated into plasma and peripheral blood mononuclear cells (PBMCs) by Ficoll density centrifugation (Nacalai Tesque, Inc. Kyoto, Japan). Inguinal lymph nodes were obtained from these animals by biopsy at 2 wpi and before infection. Single-cell suspensions were prepared from the inguinal lymph nodes with a 100 μm nylon cell strainer (Becton Dickinson). Data from two monkeys (MM346 and MM349) that were inoculated with the same dose of SHIV-NI in a previous report (Shimizu et al., 2005) were also utilized. Data from four naive monkeys (MM298, MM299, MM338, and MM339) that were infected intravenously with the same dose (10^5 $TCID_{50}$) of SHIV-C2/1 KS661, were used as control (Shimizu et al., 2005).

Lymphocyte immunophenotyping

Anticoagulated whole-blood specimens or lymphocytes obtained from peripheral lymph node biopsies were immunophenotyped with the following monoclonal antibodies (MAbs): anti-CD4 (Nichirei, Tokyo, Japan), anti-CD8 (Becton Dickinson), anti-CD3 (BioSource International), anti-CD20 (Becton Dickinson), anti-CD14 (Beckman Coulter, Miami, FL), anti-CCR5 (Pharmingen, San Diego, CA), anti-CXCR4 (Pharmingen), anti-CD28 (Pharmingen), anti-CD95 (Pharmingen), anti-CD69 (Pharmingen), anti-CD80 (Pharmingen), anti-CD154 (Pharmingen), anti-CD212 (Pharmingen), and anti-HLA-DR (Pharmingen). Ten thousand events per sample were acquired by the FACSCaliber, and data were analyzed by CellQuest software (Becton Dickinson) and FlowJo software (TreeStar, San Carlos, CA). Absolute lymphocyte counts on blood specimens were obtained with an automated hematology analyzer (F-820; Sysmex, Kobe, Japan). Peripheral blood $CD4^+$ T lymphocytes counts were calculated by multiplying the total lymphocyte count by the percentage of $CD3^+CD4^+$ T cells.

Plasma viral RNA loads

Plasma viral RNA loads were determined by quantitative RT-PCR as described previously (Enose et al., 2002; Suryanarayana et al., 1998). Total RNAs were prepared from plasma with a QIAamp viral RNA kit (QIAGEN, Valencia, CA), and RT-PCR was performed using a Platinum Quantitative RT-PCR ThermoScript one-step system kit (Invitrogen Corp., Carlsbad, CA). The plasma viral loads of SHIV-NI, SHIV-RANTES, and the challenge virus were differentially evaluated with primer pairs specific to SHIV-NM3rN and SHIV-C2/1, respectively (Enose et al., 2004). These reactions were performed with a Prism 7700 Sequence Detector (Applied Biosystems, Foster City, CA) and analyzed using the manufacturer's software.

Virus isolation

To isolate the virus, $CD8^+$-depleted PBMCs were co-cultured with M8166 cells, as described previously (Enose et al., 2004). $CD8^+$-depleted PBMCs were obtained from each monkey by using mouse anti-human CD8 MAb (Nichirei, Japan) and sheep anti-mouse IgG magnetic beads (Dynabeads M-450; Dynal A. S., Oslo, Norway). Viral recovery, based on the syncytium formation, was monitored for 4 weeks.

Isolation of proviral DNA

Proviral DNA was extracted from 1×10^6 PBMCs and tissues of the inoculated monkeys. When the virus was re-isolated, $CD8^+$-depleted PBMCs, which were co-cultured with M8166 cells, were also monitored. Cellular DNAs were extracted using DNeasy tissue kits (QIAGEN). To check the stability of inserted RANTES gene in SHIV-RANTES, the proviral DNA fragments covering the inserted RANTES gene in SHIV-RANTES were amplified by PCR with primers specific for the *nef* region (Kuwata et al., 2000; Shimizu et al., 2006). The lengths of DNA fragments generated by this reaction were 415 bp for the SHIV containing the intact RANTES gene and 154 bp for SHIV-NI. The proviral DNA loads were determined by quantitative PCR. PCR was performed with a Taqman PCR reagent kit (Perkin Elmer) using the same primer and probe which were used in RT-PCR. A standard curve was generated from a plasmid DNA sample containing the full genome of SHIV-NM3rN or SHIV-C2/1 KS661, which was quantified with a UV-spectrophotometer.

Determination of plasma level of RANTES

Plasma RANTES concentration was measured using a human RANTES ELISA kit (R&D Systems, Inc., Minneapolis, MN), which is known to cross-react with rhesus RANTES (Kwofie et al., 2000). Because chemokine gene transcription can change dramatically during storage of whole blood for periods of as little as 6 h (Tanner et al., 2002), platelet-poor plasma was prepared from whole blood samples within 2 h by centrifugation at $10{,}000\times g$ for 10 min at 4 °C according to the manufacturer's recommendation. Samples that had been aliquoted and stored at −80 °C were thawed immediately before assay and were not reused.

Chemokine and cytokine mRNA analysis by real-time PCR amplification

Inguinal lymph nodes suspensions were collected from rhesus macaques at the time of biopsy. Total RNA was isolated using an RNA Mini kit (Qiagen). All samples were DNase (Qiagen)-treated for 20 min at 37 °C. cDNA was prepared using random hexamer primers (Invitrogen) and M-MLV-Reverse-Transcriptase (Super Script III, Invitrogen). Real-time PCR amplifications were conducted by SYBR Green methods. Oligonucleotide primers were designed for the TaqMan assay based on previously published reports (Abel et al., 2001; Hofmann-Lehmann et al., 2002). The following primers were

used: IFN-γ (F, GAAAAGCTGACCAATTATTCGGTAA; R, AGCCATCACTTGGATGAGTTCA), IL-2 (F, CACCAGGATGCTCACATTTAAGTT; R, GAGGTTTGAGTTCTTCTTCTAGACACTGA), IL-4 (F, AAACGGCTCGACAGGAACCT; R CTCTGGTTGGCTTCCTTCACA), IL-10 (F, CACGACCCAGACATCAAGGA; R, CCACGGCCTTGCTCTTGTT), TNF-α (F, GGCTCAGGCAGTCAGATCATC; R, GCTTGAGGGTTTGCTACAACATG), RANTES (F, ACCAGTGGCAAGTGCTCCA; R, TGGCACACACTTGGCGATT), and glyceraldehydes-3-phosphate dehydrogenase (GAPDH) (F, GCACCACCAACTGCTTAGCAC; R, TCTTCTGGGTGGCAGTGATG). Primers were used at a final concentration of 50 or 300 nM. The reaction was carried out in a 25 μl reaction volume containing appropriate diluted 5 μl of cDNA with SYBR Green PCR master Mix (Applied Biosystems). All sequences were amplified using the following amplification program: 2 min at 50 °C, 10 min at 95 °C, followed by 50 to 55 cycles of 15 s at 95 °C and 1 min at 60 °C with a Prism 7700 or 7000 Sequence Detector (Applied Biosystems). Samples were tested in duplicate, and the PCR for the housekeeping gene (GAPDH) and the target (cytokine or chemokine) gene was run in parallel on the same plate. The relative quantities of cytokine mRNA transcripts were determined by comparative threshold cycle (C_T) methods ($\Delta\Delta C_T$ methods) (Pfaffl, 2001). In this analysis, the C_T value for the housekeeping gene is subtracted from the C_T value of the target gene (ΔC_T). The target gene and the housekeeping gene were amplified with the same efficiency (data not shown). The mRNA samples from one SHIV-NI-immunized monkey, MM428, were defined as a standard. $\Delta\Delta C_T$ values were calculated as follows: $\Delta\Delta C_T = \Delta C_T$ value for each individual monkey-ΔC_T value of standard monkey. Then, the relative quantitation of cytokine mRNA expression level was calculated by $2^{-\Delta\Delta CT}$.

Proliferation assays

Lymphocyte proliferation was measured by incorporation of BrdU into the stimulated-lymphocytes (Shimizu et al., 2005). PBMCs (2×10^5) were cultured in a 96-well plate in RPMI 1640 with 10% FCS (complete RPMI medium). The recombinant viral proteins of SIV Gag (SIVmac251 p27; 5.0 μg/ml; Advanced Biotechnologies, Inc., Columbia, MD) were used for antigen-specific stimulation. Concanavalin A (ConA; 0.5 μg/ml; Sigma, St. Louis, MO) was used for polyclonal stimulation. The plates were incubated for 72 h at 37 °C. After the incubation, the cells were cultured for another 24 h in the presence of BrdU. Then lymphocyte proliferation was measured using a BrdU-Flow kit (Pharmingen) following the manufacturer's recommendations. To characterize the lymphocyte subsets in the proliferated cells, cells were stained for surface markers with MAb CD4-PE (Nichirei) and CD8-PerCP (Becton Dickinson). The cells were stained with MAb BrdU-FITC after fixation and permeabilization, and then analyzed by FACScan (Becton Dickinson). Proliferation responses to the antigens were considered positive if the stimulation index (SI = titers for antigen-stimulated samples / titers for control samples without antigens) exceeded 2.0 (Shimizu et al., 2005).

IFN-γ ELISpot

The frequency of antigen-specific IFN-γ-producing cells from PBMCs was determined by ELISpot analysis. The IFN-γ ELISpot assay was conducted according to the protocol provided by the manufacturer (Mabtech, Nacka Strand, Sweden). Briefly, 96-well Multiscreen-IP plates (Multiscreen MAIPS45-10, Millipore, Bedford, MA) were coated with 15 μg/ml anti-IFN-γ Mab in sterilized phosphate-buffered saline (PBS) overnight at 4 °C. Then, PBMCs were incubated with or without 5 μg/ml of SIV Gag for 24 h at 37 °C and were added to the pre-coated plates at 2.0 and 5.0×10^5 cells/well in complete RPMI medium. Experiments were performed in duplicate wells. PBMCs which were incubated with 0.5 μg/ml of ConA for 2 h at 37 °C were also used as a polyclonal stimulation. Plates were incubated for about 36 h at 37 °C. Following incubation, cells were removed, and residual cells were lysed with ice-cold water for 10 min. Biotinylated anti-IFN-γ monoclonal antibody was added and incubated for 3 h at room temperature, followed by addition of streptavidin-horseradish peroxidase for 2 h at room temperature. Spots were developed with a Vector *NovaRED*™ Substrate kit for peroxidase (Vector Labs, CA). The number of spot-forming cells was determined by using a light microscope. The average number of spots present in the non-stimulated cultures was subtracted from the average number in the antigen-stimulated cultures.

Determination of anti-SHIV antibody titers

Anti-SHIV antibody titers in the plasma of the monkeys were determined using a commercial particle agglutination test kit (Genedia HIV-1/2, Fujirebio Inc., Tokyo, Japan). The samples were serially two-fold diluted and assayed following the manufacturer's recommendations. The end-point titer was determined as the highest dilution to give a positive result.

Statistical analysis

Differences between the SHIV-RANTES- and SHIV-NI-inoculated monkeys were analyzed with the Mann–Whitney *U* test. *P* values <0.05 were considered statistically significant.

Acknowledgments

We thank Drs. E. Ido, Y. Endo, K. Maeda, and H. Kato for their valuable comments and suggestions, T. Kazama and W. Shinzato for technical assistance with the analyses, Drs. K. Sakai, K. Shinohara, and E. Takahashi for kindly providing SHIV-C2/1. We are grateful to J. Berline at University of California, San Francisco for carefully reading the manuscript and editing the English language. This work was supported by a Grant-in-Aid for Scientific Research from the Ministry of Education and Science, Japan, Research on HIV/AIDS in Health and labour Sciences Research Grants from the Ministry of Health, Labour and Welfare, Japan and a Research Grant on Health Sciences focusing on Drug Innovation from the Japan Health Sciences Foundation.

References

Abel, K., Alegria-Hartman, M.J., Zanotto, K., McChesney, M.B., Marthas, M.L., Miller, C.J., 2001. Anatomic site and immune function correlate with relative cytokine mRNA expression levels in lymphoid tissues of normal rhesus macaques. Cytokine 16, 191–204.

Ahmed, R.K., Nilsson, C., Wang, Y., Lehner, T., Biberfeld, G., Thorstensson, R., 1999. Beta-chemokine production in macaques vaccinated with live attenuated virus correlates with protection against simian immunodeficiency virus (SIVsm) challenge. J. Gen. Virol. 80 (Pt. 7), 1569–1574.

Alkhatib, G., Combadiere, C., Broder, C.C., Feng, Y., Kennedy, P.E., Murphy, P.M., Berger, E.A., 1996. CC CKR5: a RANTES, MIP-1alpha, MIP-1beta receptor as a fusion cofactor for macrophage-tropic HIV-1. Science 272, 1955–1958.

Baba, T.W., Liska, V., Khimani, A.H., Ray, N.B., Dailey, P.J., Penninck, D., Bronson, R., Greene, M.F., McClure, H.M., Martin, L.N., Ruprecht, R.M., 1999. Live attenuated, multiply deleted simian immunodeficiency virus causes AIDS in infant and adult macaques. Nat. Med. 5, 194–203.

Bonecchi, R., Bianchi, G., Bordignon, P.P., D'Ambrosio, D., Lang, R., Borsatti, A., Sozzani, S., Allavena, P., Gray, P.A., Mantovani, A., Sinigaglia, F., 1998. Differential expression of chemokine receptors and chemotactic responsiveness of type 1 T helper cells (Th1s) and Th2s. J. Exp. Med. 187, 129–134.

Cocchi, F., DeVico, A.L., Garzino-Demo, A., Arya, S.K., Gallo, R.C., Lusso, P., 1995. Identification of RANTES, MIP-1 alpha, and MIP-1 beta as the major HIV-suppressive factors produced by CD8+ T cells. Science 270, 1811–1815.

Enose, Y., Ui, M., Miyake, A., Suzuki, H., Uesaka, H., Kuwata, T., Kunisawa, J., Kiyono, H., Takahashi, H., Miura, T., Hayami, M., 2002. Protection by intranasal immunization of a nef-deleted, nonpathogenic SHIV against intravaginal challenge with a heterologous pathogenic SHIV. Virology 298, 306–316.

Enose, Y., Kita, M., Yamamoto, T., Suzuki, H., Miyake, A., Horiuchi, R., Ibuki, K., Kaneyasu, K., Kuwata, T., Takahashi, E., Sakai, K., Shinohara, K., Miura, T., Hayami, M., 2004. Protective effects of nef-deleted SHIV or that having IFN-gamma against disease induced with a pathogenic virus early after vaccination. Arch. Virol. 149, 1705–1720.

Frauenschuh, A., DeVico, A.L., Lim, S.P., Gallo, R.C., Garzino-Demo, A., 2004. Differential polarization of immune responses by co-administration of antigens with chemokines. Vaccine 23, 546–554.

Gauduin, M.C., Glickman, R.L., Ahmad, S., Yilma, T., Johnson, R.P., 1999. Immunization with live attenuated simian immunodeficiency virus induces strong type 1 T helper responses and beta-chemokine production. Proc. Natl. Acad. Sci. U.S.A. 96, 14031–14036.

Giavedoni, L., Ahmad, S., Jones, L., Yilma, T., 1997. Expression of gamma interferon by simian immunodeficiency virus increases attenuation and reduces postchallenge virus load in vaccinated rhesus macaques. J. Virol. 71, 866–872.

Gundlach, B.R., Lewis, M.G., Sopper, S., Schnell, T., Sodroski, J., Stahl-Hennig, C., Uberla, K., 2000. Evidence for recombination of live, attenuated immunodeficiency virus vaccine with challenge virus to a more virulent strain. J. Virol. 74, 3537–3542.

Haga, T., Kuwata, T., Ui, M., Igarashi, T., Miyazaki, Y., Hayami, M., 1998. A new approach to AIDS research and prevention: the use of gene-mutated HIV-1/SIV chimeric viruses for anti-HIV-1 live-attenuated vaccines. Microbiol. Immunol. 42, 245–251.

Heeney, J.L., Teeuwsen, V.J., van Gils, M., Bogers, W.M., De Giuli Morghen, C., Radaelli, A., Barnett, S., Morein, B., Akerblom, L., Wang, Y., Lehner, T., Davis, D., 1998. beta-chemokines and neutralizing antibody titers correlate with sterilizing immunity generated in HIV-1 vaccinated macaques. Proc. Natl. Acad. Sci. U.S.A. 95, 10803–10808.

Hofmann-Lehmann, R., Williams, A.L., Swenerton, R.K., Li, P.L., Rasmussen, R.A., Chenine, A.L., McClure, H.M., Ruprecht, R.M., 2002. Quantitation of simian cytokine and beta-chemokine mRNAs, using real-time reverse transcriptase-polymerase chain reaction: variations in expression during chronic primate lentivirus infection. AIDS Res. Hum. Retroviruses 18, 627–639.

Igarashi, T., Kuwata, T., Yamamoto, H., Moriyama, H., Ui, M., Miyazaki, Y., Hayami, M., 1998. Infectivity and immunogenicity of SIVmac/HIV-1 chimeric viruses (SHIVs) with deletions in two or three genes (vpr, nef and vpx). Microbiol. Immunol. 42, 71–74.

Imami, N., Pires, A., Hardy, G., Wilson, J., Gazzard, B., Gotch, F., 2002. A balanced type 1/type 2 response is associated with long-term nonprogressive human immunodeficiency virus type 1 infection. J. Virol. 76, 9011–9023.

Johnson, R.P., Desrosiers, R.C., 1998. Protective immunity induced by live attenuated simian immunodeficiency virus. Curr. Opin. Immunol. 10, 436–443.

Kalams, S.A., Walker, B.D., 1998. The critical need for CD4 help in maintaining effective cytotoxic T lymphocyte responses. J. Exp. Med. 188, 2199–2204.

Kim, J.J., Nottingham, L.K., Sin, J.I., Tsai, A., Morrison, L., Oh, J., Dang, K., Hu, Y., Kazahaya, K., Bennett, M., Dentchev, T., Wilson, D.M., Chalian, A.A., Boyer, J.D., Agadjanyan, M.G., Weiner, D.B., 1998. CD8 positive T cells influence antigen-specific immune responses through the expression of chemokines. J. Clin. Invest. 102, 1112–1124.

Kinter, A., Catanzaro, A., Monaco, J., Ruiz, M., Justement, J., Moir, S., Arthos, J., Oliva, A., Ehler, L., Mizell, S., Jackson, R., Ostrowski, M., Hoxie, J., Offord, R., Fauci, A.S., 1998. CC-chemokines enhance the replication of T-tropic strains of HIV-1 in CD4(+) T cells: role of signal transduction. Proc. Natl. Acad. Sci. U.S.A. 95, 11880–11885.

Koff, W.C., Johnson, P.R., Watkins, D.I., Burton, D.R., Lifson, J.D., Hasenkrug, K.J., McDermott, A.B., Schultz, A., Zamb, T.J., Boyle, R., Desrosiers, R.C., 2006. HIV vaccine design: insights from live attenuated SIV vaccines. Nat. Immunol. 7, 19–23.

Kuwata, T., Miura, T., Haga, T., Kozyrev, L., Hayami, M., 2000. Construction of chimeric simian and human immunodeficiency viruses that produce interleukin 12. AIDS Res. Hum. Retroviruses 16, 465–470.

Kuwata, T., Miura, T., Hayami, M., 2001. Using SHIVs to develop an anti-HIV-1 live-attenuated vaccine. Trends Microbiol. 9, 475–480.

Kwofie, T.B., Haga, T., Iida, T., Hayami, M., Miura, T., 2000. Plasma levels of the chemokine RANTES in macaque monkeys infected with pathogenic and non-pathogenic SIV/HIV-1 chimeric viruses at an early stage of infection. J. Vet. Med. Sci. 62, 1311–1312.

Lillard Jr., J.W., Boyaka, P.N., Taub, D.D., McGhee, J.R., 2001. RANTES potentiates antigen-specific mucosal immune responses. J. Immunol. 166, 162–169.

Loetscher, P., Uguccioni, M., Bordoli, L., Baggiolini, M., Moser, B., Chizzolini, C., Dayer, J.M., 1998. CCR5 is characteristic of Th1 lymphocytes. Nature 391, 344–345.

Luster, A.D., 1998. Chemokines-chemotactic cytokines that mediate inflammation. N. Engl. J. Med. 338, 436–445.

Matloubian, M., Concepcion, R.J., Ahmed, R., 1994. CD4+ T cells are required to sustain CD8+ cytotoxic T-cell responses during chronic viral infection. J. Virol. 68, 8056–8063.

Miller, C.J., Abel, K., 2005. Immune mechanisms associated with protection from vaginal SIV challenge in rhesus monkeys infected with virulence-attenuated SHIV 89.6. J. Med. Primatol. 34, 271–281.

Pfaffl, M.W., 2001. A new mathematical model for relative quantification in real-time RT-PCR. Nucleic Acids Res. 29, e45.

Proudfoot, A.E., Wells, T.N., Clapham, P.R., 1999. Chemokine receptors-future therapeutic targets for HIV? Biochem. Pharmacol. 57, 451–463.

Rosenberg, E.S., Billingsley, J.M., Caliendo, A.M., Boswell, S.L., Sax, P.E., Kalams, S.A., Walker, B.D., 1997. Vigorous HIV-1-specific CD4+ T cell responses associated with control of viremia. Science 278, 1447–1450.

Rosenberg, E.S., Altfeld, M., Poon, S.H., Phillips, M.N., Wilkes, B.M., Eldridge, R.L., Robbins, G.K., D'Aquila, R.T., Goulder, P.J., Walker, B.D., 2000. Immune control of HIV-1 after early treatment of acute infection. Nature 407, 523–526.

Sallusto, F., Lanzavecchia, A., Mackay, C.R., 1998. Chemokines and chemokine receptors in T-cell priming and Th1/Th2-mediated responses. Immunol. Today 19, 568–574.

Schmittel, A., Keilholz, U., Scheibenbogen, C., 1997. Evaluation of the interferon-gamma ELISPOT-assay for quantification of peptide specific T lymphocytes from peripheral blood. J. Immunol. Methods 210, 167–174.

Shimizu, Y., Miyazaki, Y., Ibuki, K., Suzuki, H., Kaneyasu, K., Goto, Y., Hayami, M., Miura, T., Haga, T., 2005. Induction of immune response in macaque monkeys infected with simian–human immunodeficiency virus

having the TNF-alpha gene at an early stage of infection. Virology 343, 151–161.

Shimizu, Y., Okoba, M., Yamazaki, N., Goto, Y., Miura, T., Hayami, M., Hoshino, H., Haga, T., 2006. Construction and in vitro characterization of a chimeric simian and human immunodeficiency virus with the RANTES gene. Microbes Infect. 8, 105–113.

Shinohara, K., Sakai, K., Ando, S., Ami, Y., Yoshino, N., Takahashi, E., Someya, K., Suzaki, Y., Nakasone, T., Sasaki, Y., Kaizu, M., Lu, Y., Honda, M., 1999. A highly pathogenic simian/human immunodeficiency virus with genetic changes in cynomolgus monkey. J. Gen. Virol. 80, 1231–1240.

Stahl-Hennig, C., Gundlach, B.R., Dittmer, U., ten Haaft, P., Heeney, J., Zou, W., Emilie, D., Sopper, S., Uberla, K., 2003. Replication, immunogenicity, and protective properties of live-attenuated simian immunodeficiency viruses expressing interleukin-4 or interferon-gamma. Virology 305, 473–485.

Suryanarayana, K., Wiltrout, T.A., Vasquez, G.M., Hirsch, V.M., Lifson, J.D., 1998. Plasma SIV RNA viral load determination by real-time quantification of product generation in reverse transcriptase-polymerase chain reaction. AIDS Res. Hum. Retroviruses 14, 183–189.

Tanner, M.A., Berk, L.S., Felten, D.L., Blidy, A.D., Bit, S.L., Ruff, D.W., 2002. Substantial changes in gene expression level due to the storage temperature and storage duration of human whole blood. Clin. Lab. Haematol. 24, 337–341.

Taub, D.D., Ortaldo, J.R., Turcovski-Corrales, S.M., Key, M.L., Longo, D.L., Murphy, W.J., 1996. Beta chemokines costimulate lymphocyte cytolysis, proliferation, and lymphokine production. J. Leukocyte Biol. 59, 81–89.

Ui, M., Kuwata, T., Igarashi, T., Ibuki, K., Miyazaki, Y., Kozyrev, I.L., Enose, Y., Shimada, T., Uesaka, H., Yamamoto, H., Miura, T., Hayami, M., 1999. Protection of macaques against a SHIV with a homologous HIV-1 Env and a pathogenic SHIV-89.6P with a heterologous Env by vaccination with multiple gene-deleted SHIVs. Virology 265, 252–263.

Waterman, P.M., Kitabwalla, M., Hatfield, G.S., Evans, P.S., Lu, Y., Tikhonov, I., Bryant, J.L., Pauza, C.D., 2004. Effects of virus burden and chemokine expression on immunity to SHIV in nonhuman primates. Viral Immunol. 17, 545–557.

Xin, K.Q., Lu, Y., Hamajima, K., Fukushima, J., Yang, J., Inamura, K., Okuda, K., 1999. Immunization of RANTES expression plasmid with a DNA vaccine enhances HIV-1-specific immunity. Clin. Immunol. 92, 90–96.

JOURNAL OF VIROLOGY, June 2008, p. 6039–6044 Vol. 82, No. 12
0022-538X/08/$08.00+0 doi:10.1128/JVI.02753-07

Small Intestine CD4$^+$ T Cells Are Profoundly Depleted during Acute Simian-Human Immunodeficiency Virus Infection, Regardless of Viral Pathogenicity$^\nabla$

Yoshinori Fukazawa,[1]† Ariko Miyake,[1,2]† Kentaro Ibuki,[1] Katsuhisa Inaba,[1] Naoki Saito,[1] Makiko Motohara,[1] Reii Horiuchi,[1] Ai Himeno,[1] Kenta Matsuda,[1] Megumi Matsuyama,[1] Hidemi Takahashi,[3] Masanori Hayami,[1] Tatsuhiko Igarashi,[1] and Tomoyuki Miura[1]*

Laboratory of Primate Model, Experimental Research Center for Infectious Diseases, Institute for Virus Research, Kyoto University, 53 Shogoinkawaramachi, Sakyo-ku, Kyoto 606-8507, Japan[1]; Laboratory of Tumor Cell Biology, Department of Medical Genome Sciences, Graduate School of Frontier Sciences, The University of Tokyo, Tokyo 162-8640, Japan[2]; and Department of Microbiology and Immunology, Nippon Medical School, Tokyo 113-8602, Japan[3]

Received 27 December 2007/Accepted 27 March 2008

To analyze the relationship between acute virus-induced injury and the subsequent disease phenotype, we compared the virus replication and CD4$^+$ T-cell profiles for monkeys infected with isogenic highly pathogenic (KS661) and moderately pathogenic (#64) simian-human immunodeficiency viruses (SHIVs). Intrarectal infusion of SHIV-KS661 resulted in rapid, systemic, and massive virus replication, while SHIV-#64 replicated more slowly and reached lower titers. Whereas KS661 systemically depleted CD4$^+$ T cells, #64 caused significant CD4$^+$ T-cell depletion only in the small intestine. We conclude that SHIV, regardless of pathogenicity, can cause injury to the small intestine and leads to CD4$^+$ T-cell depletion in infected animals during acute infection.

The highly pathogenic simian-human immunodeficiency virus (SHIV) SHIV-C2/1-KS661 (KS661), which was derived from SHIV-89.6 (23), replicates to high titers and causes the irreversible depletion of the circulating CD4$^+$ T cells during the acute phase of intravenous infection, followed by AIDS-like disease within 1 year (23). We previously reported that KS661 massively replicates and depletes CD4$^+$ T cells in both peripheral and mucosal lymphoid tissues during the initial 4 weeks postinfection (16). On the other hand, the isogenic SHIV-#64 (#64), which was derived from SHIV-89.6P, is moderately pathogenic. The genomic sequences of the two SHIVs differ by only 0.16%, resulting in a total of six amino acid changes in the products of the *pol*, *env-gp41*, and *rev* genes. The intravenous inoculation of rhesus macaques with #64 induces plasma viral burdens comparable to those induced by KS661 during the acute phase of infection and causes a transient reduction of the circulating CD4$^+$ T lymphocytes (10). After the acute phase, the viral loads decline to undetectable levels and the populations of CD4$^+$ T cells recover to preinfection levels.

To clarify the relationship between acute viral replication kinetics and subsequent clinical courses for these isogenic SHIVs with distinct pathogenicities, we examined proviral DNA, infectious-virus-producing cells (IVPCs), and CD4$^+$ T-cell depletion in peripheral and mucosal lymphoid tissues of 17 infected (Table 1) and 7 uninfected adult rhesus macaques (*Macaca mulatta*). Both Chinese and Indian rhesus monkeys were randomly assigned to these groups. The monkeys were used in accordance with the institutional regulations approved by the Committee for Experimental Use of Nonhuman Primates of the Institute for Virus Research, Kyoto University, Kyoto, Japan. The animals were inoculated via intrarectal infusion as described previously (17). Following serial euthanasia, tissues were collected and analyzed up to 27 days postinfection (dpi) as described previously (16, 17).

Gross virus replication was assessed by measuring plasma viral loads by reverse transcriptase PCR (16). By 6 dpi, plasma viral RNA levels became detectable in all the KS661-infected macaques (Fig. 1A) and three of seven #64-infected macaques (animals MM372, MM391, and MM374) (Fig. 1B). Although the plasma viral loads of the two groups at 13 dpi, when the virus loads reached their initial peaks, were not significantly different ($P = 0.1673$), the average load (± the standard deviation) in KS661-infected monkeys ($9.3 \times 10^8 \pm 15.9 \times 10^8$ copies/ml) was about 10 times higher than that in #64-infected monkeys ($6.3 \times 10^7 \pm 11.6 \times 10^7$ copies/ml). These results suggest that KS661 spread faster and reached a somewhat higher titer than did #64 when the viruses were inoculated intrarectally.

Levels of peripheral blood CD4$^+$ T lymphocytes in all the KS661-infected monkeys decreased substantially within 4 weeks (Fig. 1C). On the other hand, the reductions in the levels of CD4$^+$ T cells varied among the #64-infected monkeys (Fig. 1D). For example, MM378 did not exhibit any appreciable changes, even though the plasma viral RNA load in this monkey reached 2.6×10^7 copies/ml by 21 dpi (Fig. 1 B and D).

* Corresponding author. Mailing address: Laboratory of Primate Model, Experimental Research Center for Infectious Diseases, Institute for Virus Research, Kyoto University, 53 Shogoinkawaramachi, Sakyo-ku, Kyoto 606-8507, Japan. Phone: 81-75-751-3984. Fax: 81-75-761-9335. E-mail: tmiura@virus.kyoto-u.ac.jp.
† These authors contributed equally to this work.
▽ Published ahead of print on 9 April 2007.

TABLE 1. Experimental schedule for individual monkeys[a]

Virus (inoculum size)	Monkeys examined at:		
	6 dpi	13 dpi	27 dpi
KS661 (2×10^5 $TCID_{50}$)	MM300, MM309	MM313, MM334, MM392, MM393	MM308, MM310, MM394, MM395
#64 (2×10^5 $TCID_{50}$)	MM379, MM390	MM372, MM373*, MM391	MM374, MM378

[a] $TCID_{50}$, 50% tissue culture infective doses; *, MM373 received 2×10^3 $TCID_{50}$ of #64.

These data suggest that the decline in circulating $CD4^+$ T cells in KS661-infected animals was more severe and more reproducible than that in the #64-infected monkeys.

Another highly pathogenic SHIV, SHIV-DH12R, is known to cause systemic and synchronous replication events in animals following intravenous inoculation (6). To reveal the spread of virus in monkeys following intrarectal infection, we measured proviral DNA loads in a variety of tissues as described previously (16). KS661 proviral DNA was detected not only in samples from the rectums, the site of virus inoculation, but also in peripheral blood mononuclear cells and some lymph nodes (LN) at 6 dpi (Fig. 2A), suggesting that the virus was already spreading systemically. At 13 dpi, when the viral RNA loads in peripheral blood increased to the highest titers, proviral DNA levels in all of the tissues examined also increased, with levels in most monkeys exceeding 10^4 copies/μg of DNA. The levels of proviral DNA in all the tissues declined remarkably by 27 dpi. In contrast, #64 proviral DNA was detected only in the rectum of one (MM390) of the two monkeys examined at 6 dpi (Fig. 2A). At 13 dpi, the amount of proviral DNA in each tissue sample from #64-infected monkeys ($<10^4$ copies/μg of DNA) was considerably smaller than

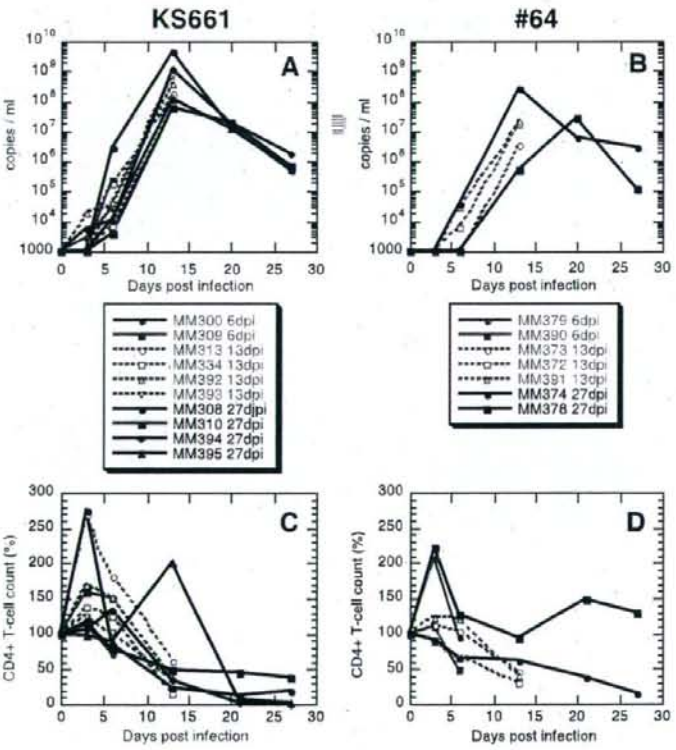

FIG. 1. Plasma viral RNA loads and profiles of circulating $CD4^+$ T cells for monkeys intrarectally infected with highly pathogenic KS661 and moderately pathogenic #64. (A and B) Plasma viral RNA loads were measured by quantitative reverse transcriptase PCR. The detection limit of this assay was 10^3 copies/ml. (C and D) Levels of $CD4^+$ T cells in peripheral blood samples from monkeys infected with KS661 and #64. The absolute number of $CD3^+$ $CD4^+$ cells in peripheral blood immediately before infection (day 0 postinfection) was defined as 100% for each monkey.

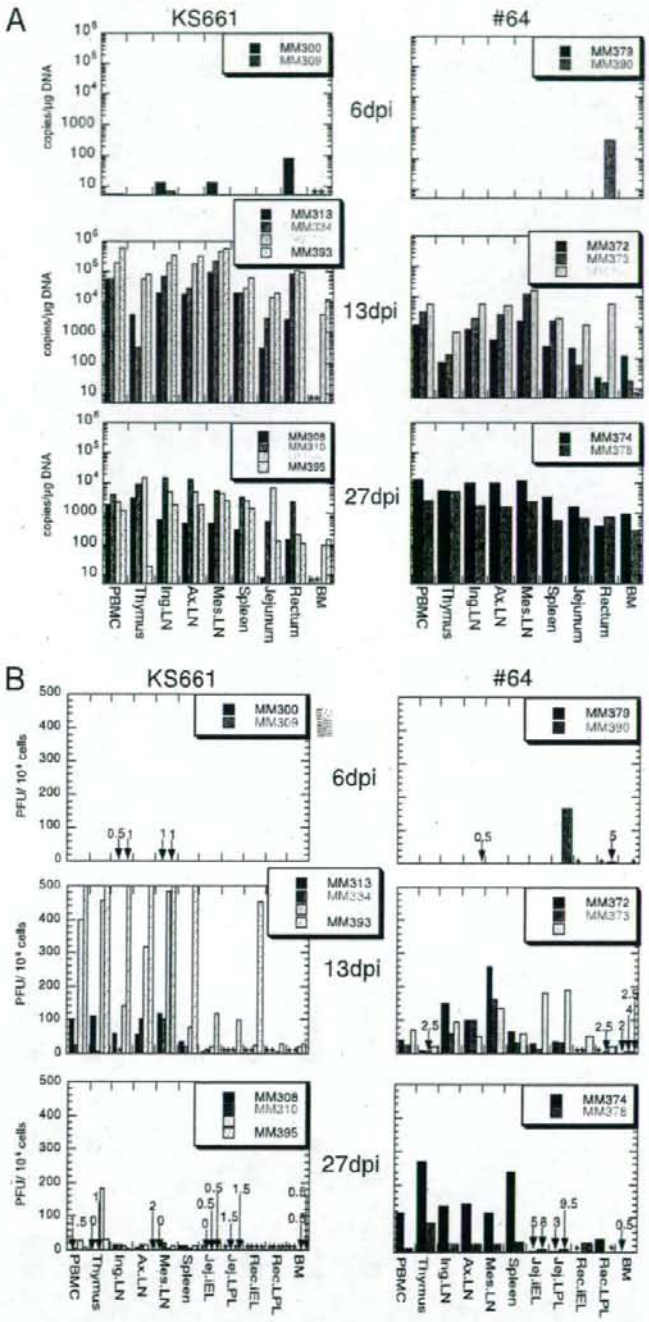

FIG. 2. (A) Proviral DNA loads in tissues of KS661- and #64-infected monkeys at 6, 13, and 27 dpi. Viral burdens were determined by quantitative PCR and expressed as the numbers of viral DNA copies per microgram of total DNA extracted from tissue homogenates. PBMC, peripheral blood mononuclear cells; Ing., inguinal; Ax., axillary; Mes., mesenteric; BM, bone marrow; *, not done. (B) Numbers of IVPCs in tissues of KS661- and #64-infected monkeys at 6, 13, and 27 dpi. Numbers of IVPCs were determined by an infectious plaque assay and were expressed as the numbers of PFU per 10^6 cells. Jej., jejunum; Rec., rectum; iEL, intraepithelial lymphocytes; *, not done.

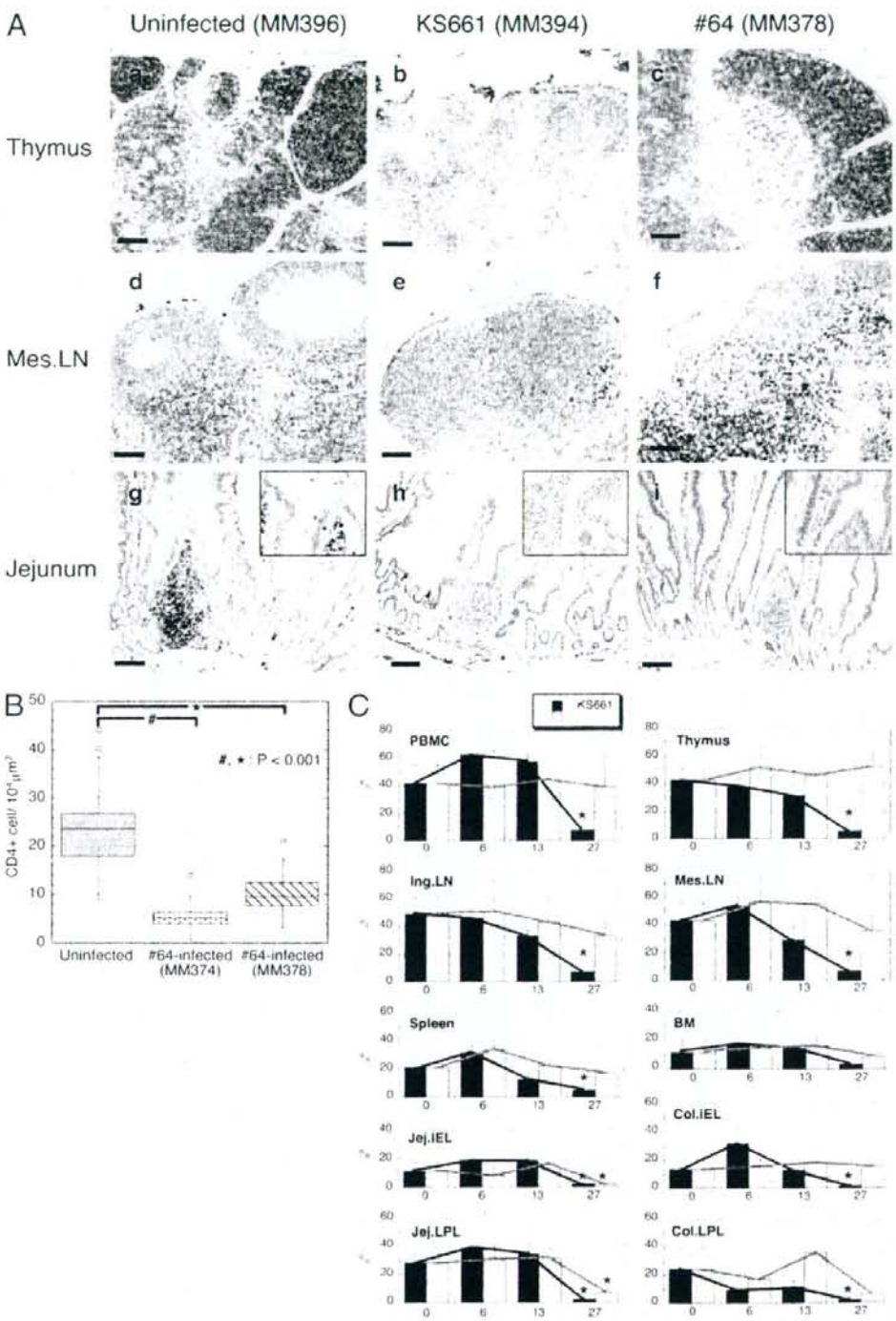

that in each sample from the KS661-infected monkeys. However, unlike the KS661 proviral DNA levels, the #64 proviral DNA levels in most tissues were maintained up to 27 dpi. These results suggest that #64 spread more slowly than KS661 and that the amounts of proviral DNA in a variety of tissues from the #64-infected animals were smaller than those in the tissues from KS661-infected animals around the initial peak of plasma viremia.

Because the amount of proviral DNA measured by PCR may include nonreplicating remnants of the viral genome, we also measured the number of IVPCs in each tissue sample by a plaque assay as described previously (9, 15). Briefly, cells prepared from infected animals were mixed with human T-lymphoid M8166 indicator cells, resuspended in culture medium containing 0.4% agarose, and plated into petri dishes. The plaques that formed in the cell layer were counted after 10 days of cultivation, and the number of IVPCs was calculated. For the KS661-infected monkeys, high numbers of IVPCs in all the tissue samples examined at 13 dpi were detected (Fig. 2B). Among these samples, the thymus and mesenteric LN samples harbored especially high numbers of IVPCs (more than 500/10^6 cells) at 13 dpi. The numbers of IVPCs declined remarkably from 13 to 27 dpi. We concluded that KS661 replicated systemically and synchronously in a variety of tissues, including the intestinal tract, at 13 dpi. In contrast, #64 production patterns in different tissues were not synchronous. Among #64-infected monkeys at 6 dpi, virus production was most active in the jejunum lamina propria lymphocytes (LPL) of MM390 (166 IVPCs/10^6 cells). At 13 dpi, interestingly, mesenteric LN became the center of virus production in two of the three monkeys examined (MM372 and MM373: 259 and 160 IVPCs/10^6 cells). In the other monkey (MM391), the jejunum had the highest number of IVPCs, followed by the mesenteric LN. These results suggested that the virus that replicated in the jejunum spread directly into the mesenteric LN via the flow of lymphatic fluid. At 27 dpi, the thymus tissues of both monkeys examined (MM374 and MM378) exhibited the highest numbers of IVPCs. In summary, the systemic dissemination of #64 was slower than that of KS661, and it was particularly delayed in the thymus during the acute phase.

Systemic $CD4^+$ cell depletion is the signature of disease induced by highly pathogenic SHIVs (7, 8, 22). We therefore compared the frequencies of $CD4^+$ cells in tissues from the animals infected with KS661 and #64, in addition to those of the circulating $CD4^+$ T lymphocytes. As representatives of the major virus-producing organs, the thymus, the mesenteric LN, and the jejunum were selected for examination. CD4 cell numbers were measured by immunohistochemistry analyses as described previously (18). Uninfected thymus tissue contained abundant $CD4^+$ cells that were stained brown (Fig. 3A, panel a), while the tissue collected from the KS661-infected animal at 27 dpi harbored few such cells (Fig. 3A, panel b). #64 caused virtually no $CD4^+$ cell depletion in the thymus at 27 dpi (Fig. 3A, panel c). In the mesenteric LN of uninfected monkeys, $CD4^+$ cells were found in the paracortical region (Fig. 3A, panel d). KS661 depleted $CD4^+$ cells in this area (Fig. 3A, panel e). Unlike KS661, #64 did not reduce the level of $CD4^+$ cells (Fig. 3A, panel f). The jejunum samples from uninfected animals contained $CD4^+$ cells in the lamina propria and follicles of gut-associated lymphatic tissues (Fig. 3 A, panel g). KS661 depleted $CD4^+$ cells in these tissues, too (Fig. 3A, panel h). Interestingly, #64 caused $CD4^+$ cell depletion in the small intestine comparable to that caused by KS661 (Fig. 3A, panel i). To confirm the observed cell reduction in the jejunum samples, we randomly selected a total of 40 fields on the tissue sections from each animal for viewing at a total magnification of ×400, counted $CD4^+$ cells, and averaged the numbers (Fig. 3B). The $CD4^+$ cell densities in the jejunum samples from the #64-infected monkeys were significantly lower than those in the samples from uninfected animals ($P < 0.001$). This gut-specific $CD4^+$ cell depletion caused by #64 prompted us to analyze the frequencies of $CD4^+$ T cells (including CD4 and CD8 doubly positive cells) in a variety of tissues by flow cytometry (Fig. 3C). KS661 caused systemic $CD4^+$ T-lymphocyte depletion by 27 dpi (Fig. 3C). In agreement with the immunohistochemistry results, #64 significantly depleted $CD4^+$ T cells only in the jejunum intraepithelial lymphocytes and LPL ($P = 0.01$ and 0.003, respectively) (Fig. 3C) by 27 dpi, although we examined only two #64-infected monkeys at 27 dpi. In conclusion, the $CD4^+$ T-cell depletion patterns caused by KS661 and #64 were distinct, and the small intestine was the only site in which $CD4^+$ T cells were significantly depleted by the moderately pathogenic #64.

Taken together, our results show that #64 disseminated more slowly and replicated less than KS661 in systemic lymphoid tissues, as well as in peripheral blood, during the acute phase of infection. We believe that because of its low rate and low levels of replication, #64 could not cause irreversible injury before the host mounted an immune reaction. As a result, $CD4^+$ T cells were not completely depleted in all the tissues examined, except in the small intestine. These results suggest that the small intestine is the tissue most sensitive to virus-induced $CD4^+$ T-cell depletion during the acute phase of infection. Recent reports revealed that severe acute depletions

FIG. 3. Profiles of $CD4^+$ T cells in systemic lymphoid tissues during acute infection. (A) Immunohistochemical staining for CD4 molecules (stained brown) in the thymus, mesenteric (mes.) LN, and jejunum tissues of KS661- or #64-infected monkeys at 27 dpi, in addition to those of uninfected monkeys. Black scale bars, 100 μm; white scale bars in insets of panels g, h, and i, 50 μm. (B) Comparison of $CD4^+$ cell frequencies in the jejunum LPL of uninfected and #64-infected monkeys at 27 dpi. A total of forty randomly selected fields (total magnification, ×400) of at least four tissue sections per animal were used for the analysis of jejunum LPL. *P* values (determined by Student's *t* test with 95% confidence intervals) are for comparisons of each #64-infected monkey with uninfected monkeys. (C) Percentages of $CD4^+$ T cells among total lymphocytes from KS661- and #64-infected monkeys. In each graph, data for 0 dpi (time points postinfection are shown along the *x* axis) are averages of percentages for seven uninfected control monkeys. Percentages of $CD4^+$ T cells (including CD4 and CD8 doubly positive cells) were obtained by first gating lymphocytes and then $CD3^+$ T cells with a flow cytometer. PBMC, peripheral blood mononuclear cells; Ing., inguinal; Jej., jejunum; iEL, intraepithelial lymphocytes; BM, bone marrow; Col., colon; *, $P < 0.05$ (percentage at 0 dpi versus that at 27 dpi; Student's *t* test with a 95% confidence interval).

of mucosal CD4+ T cells have been observed in simian immunodeficiency virus-infected monkeys (11, 12, 24, 25) and human immunodeficiency virus-infected humans (2, 5, 13). The acute depletion of mucosal CD4+ T cells and the disease outcome are correlated (1, 3, 21, 26). However, a decrease of mucosal CD4+ T cells has also been observed in the early phases of natural host infections, such as SIVagm infection in African green monkeys and SIVsmm infection in sooty mangabeys, which typically do not progress to AIDS (4, 14, 19). In addition, the levels of apoptosis and immune activation and the degrees of CD4+ T-cell restoration differ between progressors and nonprogressors in simian immunodeficiency virus models (4, 14, 19). Taken together, these results raise the possibility that the severe acute depletion of mucosal CD4+ T cells is not sufficient to induce AIDS. The restoration of CD4+ T cells and normal immune function after the severe acute depletion may define the eventual disease outcome (20). The abilities of KS661- and #64-infected monkeys to restore the immune system may be different, because KS661, but not #64, impairs thymic T-cell differentiation (18). Currently, we are focusing on the restoration of CD4+ T cells and the functional aspect of the immune cells in the small intestines of animals infected with KS661 and #64 to further clarify the determinant(s) of the disease outcome.

We are grateful to James Raymond for English editing of the manuscript and to Takahito Kazama for technical support.

This work was supported, in part, by Research on Human Immunodeficiency Virus/AIDS in Health and Labor Sciences research grants from the Ministry of Health, Labor and Welfare, Japan, a grant-in-aid for scientific research from the Ministry of Education and Science, Japan, a research grant for health sciences focusing on drug innovation for AIDS from the Japan Health Sciences Foundation, and a grant from the Program for the Promotion of Fundamental Studies in Health Sciences of the National Institute of Biomedical Innovation (NIBIO) of Japan.

REFERENCES

1. **Brenchley, J. M., D. A. Price, and D. C. Douek.** 2006. HIV disease: fallout from a mucosal catastrophe? Nat. Immunol. **7**:235–239.
2. **Brenchley, J. M., T. W. Schacker, L. E. Ruff, D. A. Price, J. H. Taylor, G. J. Beilman, P. L. Nguyen, A. Khoruts, M. Larson, A. T. Haase, and D. C. Douek.** 2004. CD4+ T cell depletion during all stages of HIV disease occurs predominantly in the gastrointestinal tract. J. Exp. Med. **200**:749–759.
3. **Chase, A., Y. Zhou, and R. F. Siliciano.** 2006. HIV-1-induced depletion of CD4+ T cells in the gut: mechanism and therapeutic implications. Trends Pharmacol. Sci. **27**:4–7.
4. **Gordon, S. N., N. R. Klatt, S. E. Bosinger, J. M. Brenchley, J. M. Milush, J. C. Engram, R. M. Dunham, M. Paiardini, S. Klucking, A. Danesh, E. A. Strobert, C. Apetrei, I. V. Pandrea, D. Kelvin, D. C. Douek, S. I. Staprans, D. L. Sodora, and G. Silvestri.** 2007. Severe depletion of mucosal CD4+ T cells in AIDS-free simian immunodeficiency virus-infected sooty mangabeys. J. Immunol. **179**:3026–3034.
5. **Guadalupe, M., E. Reay, S. Sankaran, T. Prindiville, J. Flamm, A. McNeil, and S. Dandekar.** 2003. Severe CD4+ T-cell depletion in gut lymphoid tissue during primary human immunodeficiency virus type 1 infection and substantial delay in restoration following highly active antiretroviral therapy. J. Virol. **77**:11708–11717.
6. **Igarashi, T., C. R. Brown, R. A. Byrum, Y. Nishimura, Y. Endo, R. J. Plishka, C. Buckler, A. Buckler-White, G. Miller, V. M. Hirsch, and M. A. Martin.** 2002. Rapid and irreversible CD4+ T-cell depletion induced by the highly pathogenic simian/human immunodeficiency virus SHIV(DH12R) is systemic and synchronous. J. Virol. **76**:379–391.
7. **Igarashi, T., Y. Endo, G. Englund, R. Sadjadpour, T. Matano, C. Buckler, A. Buckler-White, R. Plishka, T. Theodore, R. Shibata, and M. A. Martin.** 1999. Emergence of a highly pathogenic simian/human immunodeficiency virus in a rhesus macaque treated with anti-CD8 mAb during a primary infection with a nonpathogenic virus. Proc. Natl. Acad. Sci. USA **96**:14049–14054.
8. **Joag, S. V., Z. Li, L. Foresman, E. B. Stephens, L.-J. Zhao, I. Adany, D. M. Pinson, H. M. McClure, and O. Narayan.** 1996. Chimeric simian/human immunodeficiency virus that causes progressive loss of CD4+ T cells and AIDS in pig-tailed macaques. J. Virol. **70**:3189–3197.
9. **Kato, S., Y. Hiraishi, N. Nishimura, T. Sugita, M. Tomihama, and T. Takano.** 1998. A plaque hybridization assay for quantifying and cloning infectious human immunodeficiency virus type 1 virions. J. Virol. Methods **72**:1–7.
10. **Kozyrev, I. L., K. Ibuki, T. Shimada, T. Kuwata, T. Takemura, M. Hayami, and T. Miura.** 2001. Characterization of less pathogenic infectious molecular clones derived from acute-pathogenic SHIV-89.6p stock virus. Virology **282**:6–13.
11. **Li, Q., L. Duan, J. D. Estes, Z. M. Ma, T. Rourke, Y. Wang, C. Reilly, J. Carlis, C. J. Miller, and A. T. Haase.** 2005. Peak SIV replication in resting memory CD4+ T cells depletes gut lamina propria CD4+ T cells. Nature **434**:1148–1152.
12. **Mattapallil, J. J., D. C. Douek, B. Hill, Y. Nishimura, M. Martin, and M. Roederer.** 2005. Massive infection and loss of memory CD4+ T cells in multiple tissues during acute SIV infection. Nature **434**:1093–1097.
13. **Mehandru, S., M. A. Poles, K. Tenner-Racz, A. Horowitz, A. Hurley, C. Hogan, D. Boden, P. Racz, and M. Markowitz.** 2004. Primary HIV-1 infection is associated with preferential depletion of CD4+ T lymphocytes from effector sites in the gastrointestinal tract. J. Exp. Med. **200**:761–770.
14. **Milush, J. M., J. D. Reeves, S. N. Gordon, D. Zhou, A. Muthukumar, D. A. Kosub, E. Chacko, L. D. Giavedoni, C. C. Ibegbu, K. S. Cole, J. L. Miamidian, M. Paiardini, A. P. Barry, S. I. Staprans, G. Silvestri, and D. L. Sodora.** 2007. Virally induced CD4+ T cell depletion is not sufficient to induce AIDS in a natural host. J. Immunol. **179**:3047–3056.
15. **Miyake, A., Y. Enose, S. Ohkura, H. Suzuki, T. Kuwata, T. Shimada, S. Kato, O. Narayan, and M. Hayami.** 2004. The quantity and diversity of infectious viruses in various tissues of SHIV-infected monkeys at the early and AIDS stages. Arch. Virol. **149**:943–955.
16. **Miyake, A., K. Ibuki, Y. Enose, H. Suzuki, R. Horiuchi, M. Motohara, N. Saito, T. Nakasone, M. Honda, T. Watanabe, T. Miura, and M. Hayami.** 2006. Rapid dissemination of a pathogenic simian/human immunodeficiency virus to systemic organs and active replication in lymphoid tissues following intrarectal infection. J. Gen. Virol. **87**:1311–1320.
17. **Miyake, A., K. Ibuki, H. Suzuki, R. Horiuchi, N. Saito, M. Motohara, M. Hayami, and T. Miura.** 2005. Early virological events in various tissues of newborn monkeys after intrarectal infection with pathogenic simian human immunodeficiency virus. J. Med. Primatol. **34**:294–302.
18. **Motohara, M., K. Ibuki, A. Miyake, Y. Fukazawa, K. Inaba, H. Suzuki, K. Masuda, N. Minato, H. Kawamoto, T. Nakasone, M. Honda, M. Hayami, and T. Miura.** 2006. Impaired T-cell differentiation in the thymus at the early stages of acute pathogenic chimeric simian-human immunodeficiency virus (SHIV) infection in contrast to less pathogenic SHIV infection. Microbes Infect. **8**:1539–1549.
19. **Pandrea, I. V., R. Gautam, R. M. Ribeiro, J. M. Brenchley, I. F. Butler, M. Pattison, T. Rasmussen, P. A. Marx, G. Silvestri, A. A. Lackner, A. S. Perelson, D. C. Douek, R. S. Veazey, and C. Apetrei.** 2007. Acute loss of intestinal CD4+ T cells is not predictive of simian immunodeficiency virus virulence. J. Immunol. **179**:3035–3046.
20. **Picker, L. J.** 2006. Immunopathogenesis of AIDS virus infection. Curr. Opin. Immunol. **18**:399–405.
21. **Picker, L. J., and D. I. Watkins.** 2005. HIV pathogenesis: the first cut is the deepest. Nat. Immunol. **6**:430–432.
22. **Reimann, K. A., J. T. Li, R. Veazey, M. Halloran, I. W. Park, G. B. Karlsson, J. Sodroski, and N. L. Letvin.** 1996. A chimeric simian/human immunodeficiency virus expressing a primary patient human immunodeficiency virus type 1 isolate *env* causes an AIDS-like disease after in vivo passage in rhesus monkeys. J. Virol. **70**:6922–6928.
23. **Shinohara, K., K. Sakai, S. Ando, Y. Ami, N. Yoshino, E. Takahashi, K. Someya, Y. Suzaki, T. Nakasone, Y. Sasaki, M. Kaizu, Y. Lu, and M. Honda.** 1999. A highly pathogenic simian/human immunodeficiency virus with genetic changes in cynomolgus monkey. J. Gen. Virol. **80**:1231–1240.
24. **Smit-McBride, Z., J. J. Mattapallil, M. McChesney, D. Ferrick, and S. Dandekar.** 1998. Gastrointestinal T lymphocytes retain high potential for cytokine responses but have severe CD4+ T-cell depletion at all stages of simian immunodeficiency virus infection compared to peripheral lymphocytes. J. Virol. **72**:6646–6656.
25. **Veazey, R. S., M. DeMaria, L. V. Chalifoux, D. E. Shvetz, D. R. Pauley, H. L. Knight, M. Rosenzweig, R. P. Johnson, R. C. Desrosiers, and A. A. Lackner.** 1998. Gastrointestinal tract as a major site of CD4+ T cell depletion and viral replication in SIV infection. Science **280**:427–431.
26. **Veazey, R. S., and A. A. Lackner.** 2004. Getting to the guts of HIV pathogenesis. J. Exp. Med. **200**:697–700.

Vet Pathol 45:232–235 (2008)

Congenital Cystic Adenomatoid-like Malformation in a Cynomolgus Monkey (*Macaca fascicularis*)

S. Okabayashi, C. Ohno, M. Kato, H. Nakayama, and Y. Yasutomi

Tsukuba Primate Research Center, National Institute of Biomedical Innovation, Ibaraki, Japan (SO, CO, MK, YY); The Corporation for Production and Research of Laboratory Primates, Ibaraki, Japan (SO, CO, MK); and the Laboratory of Veterinary Pathology, Graduate School of Agricultural and Life Sciences, The University of Tokyo, Tokyo, Japan (HN)

Abstract. Congenital cystic adenomatoid malformation (CCAM) is a developmental lung abnormality characterized by abnormal proliferation of mesenchymal elements and failure of bronchiolar structures to mature, ultimately resulting in the compression of normal pulmonary tissue and mediastinal shift with rapid expansion of cysts. Although various clinical and pathologic studies of CCAM in humans exist, CCAM has yet to be reported in animals, even in nonhuman primates. In the present study, histopathologic analyses of a neonatal cynomolgus monkey that died 17 days after birth revealed that normal lung architecture was replaced by disorganized overgrowths of cysts lined with simple cuboidal epithelium. The epithelium projected a few ciliates into the air spaces and produced mucus. To our knowledge, this is the first case study describing CCAM or a CCAM-like lesion in nonhuman primates.

Key words: Congenital cystic adenomatoid malformation; cynomolgus monkey; histopathological analyses; lung.

Congenital cystic adenomatoid malformation (CCAM) is a rare fetal developmental abnormality of the lung. First described by Ch'in and Tang in 1949,[2] it is characterized by abnormal development of terminal respiratory structures, resulting in an adenomatoid proliferation of bronchiolar elements and cyst formation.[11,18,19] CCAM is observed mainly during the neonatal period and infancy and can be diagnosed prenatally by ultrasonography after 16 weeks of gestation.[9,10,13,14] CCAM lesions are believed to be a consequence of abnormal embryogenesis during the first 6 to 7 weeks of pregnacy.[18]

Stoker et al.[18,19] classified CCAM into three types based on clinical and histologic criteria. In the neonatal period, the expansion of cysts and the compression of surrounding lung parenchyma cause progressive respiratory distress.[18,19] Moreover, emphysema-related lung masses also cause dyspnea, eventually leading to death.[18,19] Fetuses with CCAM tend to be born prematurely or are stillborn.[12] Due to the severity and impact of this disorder, numerous clinical and pathologic studies in humans have focused on determining the pathologic mechanisms underlying CCAM and the clinical management of CCAM.[1,4,8,15,17] Although CCAM is well characterized in humans, CCAM or CCAM-like pathogenesis has not been reported in animals. To our knowledge, we report here the first case of CCAM in a nonhuman primate, as demonstrated through histopathologic analyses of a neonatal cynomolgus monkey.

A male cynomolgus monkey (*Macaca fascicularis*) born in our colony died naturally 17 days after birth. The animal was housed in an individual cage with its mother and maintained according to the National Institute of Biomedical Innovation rules and guidelines for experimental animal welfare. The mother monkey had the experience to raise another 6 baby monkeys. In this case, the mother monkey embraced her baby as usual, and the lactation also was observed. After birth, breeding staff members observed the baby monkey to check its health status; however, they could not find any abnormalities until 3 days before it died. Necropsy was performed. Tissues were fixed in 10% neutral-buffered formalin, processed conventionally, embedded in paraffin, cut into 3-μm–thick sections, and stained with hematoxylin and eosin. Lung tissues were also stained with periodic acid–Schiff (PAS), Alcian blue (AB), Masson's trichrome, and elastica van Gieson stains.

For immunohistochemical analyses, sections were first deparaffinized by pretreatment with 0.3% H_2O_2 solution. Next, sections underwent antigen retrieval with citric acid buffer and heating in an autoclave at 121°C for 10 minutes. Finally, sections were incubated free floating in primary antibody solution overnight at 4°C. The primary antibodies were anti-cytokeratin antibody (AE1/AE3 clone; 1:50; Dako, Glostrup, Denmark), anti-vimentin antibody (1:100; Dako), and anti–von Willebrand factor VIII antibody (1:400; Dako). Following brief washes with buffer, the sections were sequentially incubated with Polymer immunocomplex (Dako) for 30 minutes. Immunoreactive elements were visualized by treating the sections with 3-3′ diaminobenzidine tetroxide (Dojin Kagaku, Kumamoto, Japan). The sections then were counterstained with hematoxylin.

Fig. 1. Lung, 17-day-old monkey. The right lower lobe contains a 3.5 cm × 2 cm × 1 cm, thin-walled, multicystic structure filled with air. The remaining lobes were pinkish-red and showed signs of atelectasis. Bar = 5 mm.

Macroscopically, lesions were confined to the right lower pulmonary lobe. In the lesion area, we found a thin-walled multicystic structure (3.5 cm × 2 cm × 1 cm) filled with air (Fig. 1). The other pulmonary lobes were pinkish-red and showed signs of atelectasis (Fig. 1). In heart, both atria dilated with clot. Microscopically, the affected lung displayed diffuse, abnormal architecture composed of numerous large, partially collapsed air spaces. These lesions looked like adenomatoids, and air spaces were lined with simple cuboidal epithelium surrounded by connective tissue and immature cartilage (Fig. 2). Within the air spaces, we found a few ciliates (Fig. 3), and PAS stained a little mucus on a part of epithelium (Fig. 4). AB weakly stained premature cartilage. Masson trichrome stained fibrous interstices, but smooth muscles were not observed. Elastica van Gieson stained elastic fibers around the air spaces. Other lung tissues were congested and were compressed by the surrounding mass. The border between the cystic lesion and normal tissue was not clear. In liver and kidney, congestion was observed.

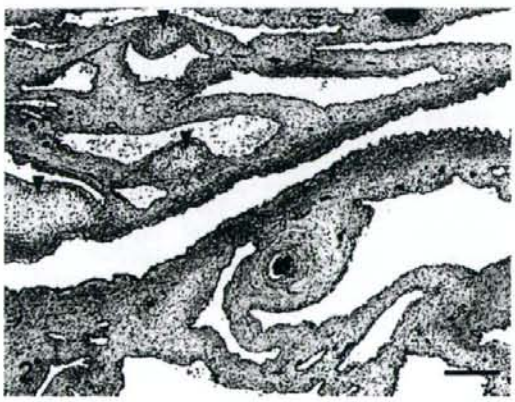

Fig. 2. Lung, 17-day-old monkey. Photomicrograph of affected lung showing diffusely abnormal architecture characterized by numerous large air spaces lined with epithelium surrounded by connective tissue and immature cartilage (arrowheads). HE. Bar = 250 μm.

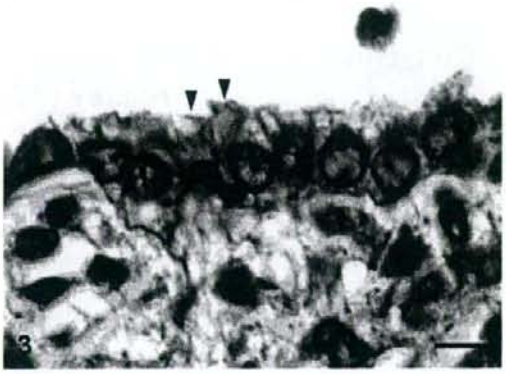

Fig. 3. Lung, 17-day-old monkey. Air spaces are lined with simple cuboidal epithelium. A few ciliated cells (arrowheads) were observed within some air spaces. HE. Bar = 6 μm.

Immunohistochemical analyses revealed that the epithelium of the lesion was immunopositive for cytokeratin but negative for vimentin and von Willebrand factor VIII. However, the fibrous interstices and premature cartilage of the lesion were immunopositive for vimentin.

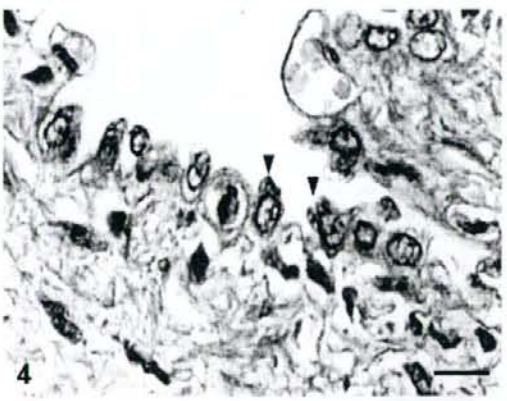

Fig. 4. Lung, 17-day-old monkey. Periodic acid–Shiff demonstrated mucus (arrowheads) on a part of the epithelium lining air spaces. Bar = 8 μm.

The congenital pulmonary abnormalities can be divided into some classifications.[5,6]

1. Bronchopulmonary sequestration:[5,6] bronchopulmonary sequestration is a pulmonary malformation in which a portion of lung parenchyma has no communication with the tracheobronchial tree and receives its blood supply via a systemic artery. The abnormality is observed as intralobar or extralobar. The first type (intralobar sequestration [ILS]) is contiguous with normal lung parenchyma and within the same visceral pleural envelope. The abnormal tissue is usually well demarcated from surrounding lung parenchyma and consists of one or more cystic spaces filled with mucus or pus. Microscopically, they resemble dilated bronchi, with respiratory epithelium and occasional mural cartilage plates. The latter type (extralobar sequestration [ELS]) is enclosed within its own pleural membrane, usually close to a normal lung. In addition to these types, the bronchopulmonary foregut malformation (BPFM)[7] is characterized by the pulmonary sequestrations that communicate with the upper gastrointestinal tract.

2. Bronchogenic cysts:[5,6] Bronchogenic cysts are lesions of congenital origin derived from the primitive foregut and are usually solitary, thin-walled, unilocular, and roughly spherical. They are filled with either mucus or serous fluid, and they do not communicate with the trancheobronchial tree. Microscopically, the cyst wall is lined by respiratory epithelium and contains cartilage, smooth muscle and, sometimes, seromucinous bronchial-type glands.

3. Congenital lobar emphysema (CLE):[5,6] CLE is characterized by severe overinflation of a pulmonary lobe. The pathogenesis is perhaps due to hypoplasia of bronchial cartilage. Microscopically, there is massive distention of alveolar spaces, but not tissue destruction.

4. Congenital cystic adenomatoid malformation (CCAM):[3,5,6,18,19] CCAM consists of an intralobar mass of disorganized pulmonary tissue that can exist with or without gross cyst formation. The anomaly is considered by some to represent a hamartoma, whereas others feel that it results from localized arrested development of the fetal bronchial tree. The cysts can usually be shown to communicate with normal airways; vascularization is by way of the pulmonary circulation. The histologic appearances give rise to the name, as there are numerous spaces of varying size, some of which resemble glandular acini, being lined cuboidal or columnar epithelium. According to the Stocker et al.[18,19] on the basis of 38 cases, CCAM is classified into three categories. Type I consists of some large cysts (>2 cm in diameter). The lesions are lined by ciliated cuboidal or columnar epithelium with elastic tissue or smooth muscle. Mucus-producing cells or cartilage may be present. Relatively normal alveoli may be seen between or adjacent to these cysts. Type II consists of small cysts (<2 cm in diameter) lacking mucus-producing cells and cartilage. Type III consists of bulky, firm, solid mass with small cysts (<0.5 cm in diameter). The lesions are lined with nonciliated cuboidal epithelium.

In this case, we found the abnormal architecture composed of numerous large air spaces. These cysts looked like adenomatoids, and they were lined with simple cuboidal epithelium surrounded by elastic tissue and premature cartilage. These pathologic features are different from that of ILS, ELS, BPFM, bronchogenic cysts, or CLE, because cysts were not unilocular, they did not include mucus or serous fluid, and they had neither abnormal artery nor communication with the upper gastrointestinal tract. Furthermore, the lesions were not massive distentions of alveolar spaces. Taken together, this monkey case is considered CCAM.

We applied the Stocker et al.[18,19] classification scheme to our monkey case, since no reports on CCAM in animals currently exist. In this monkey case, we observed large cysts greater than 2 cm in diameter (Fig. 1) lined with sparsely ciliated epithelium (Fig. 3) that produced a little mucus in a part (Fig. 4). These cysts also contained immature cartilage (Fig. 2). Thus, this monkey case exhibited sufficient pathologic features to meet the criteria for type I CCAM. We considered that pulmonary lobes were compressed by cysts and alveolars were collapsed, so that this monkey would suffer from respiratory distress and die. Moreover, the heart or great vessel may be compressed by pulmonary cysts, so that we consider liver and kidney congestion as a result of circulatory failure.

To our knowledge, this is the first case study describing CCAM or CCAM-like lesions in nonhuman primates. We have no information about the genetic background of the monkey in this case. Nonetheless, this case is quite noteworthy, because it provides an example of CCAM-like pathology in animal tissue. Should we encounter other CCAM-resembling or suspicious cases, we will carry out not only histopathologic analyses but also genetic analyses to determine the genetic background of these monkeys. Accumulating data from such analyses in nonhuman primates will contribute greatly to understanding CCAM pathology.

Acknowledgements

This study was supported by Tsukuba Primate Research Center, National Institute of Biomedical Innovation, Japan.

References

1 Bale PM: Congenital cystic malformation of the lung. A form of congenital bronchiolar ("adenomatoid") malformation. Am J Clin Pathol **71**:411–420, 1979

2 Ch'in KY, Tang MY: Congenital adenomatoid malformation of one lobe of a lung with general anasarca. Arch Pathol **48**:221–229, 1949

3 Cloutier MM, Schaeffer DA, Hight D: Congenital cystic adenomatoid malformation: review. Chest **103**:761–764, 1993

4 Dumez Y, Mandelbrot L, Radunovic N, Revillon Y, Dommergues M, Aubry MC, Aubry JP, Narcy F, Sonigo P: Prenatal management of congenital cystic adenomatoid malformation of the lung. J Pediatr Surg **28:**36–41, 1993
5 Dunnill MS: Pulmonary Pathology, Churchill Livingstone, New York, New York, 1982
6 Scarpelli EM, Auld PAM, Goldman HS, Lea, Febiger: Pulmonary Disease of the Fetus Newborn and Child, Lea & Febiger, Philadelphia, Pennsylvania, 1978
7 Eom DW, Kang GH, Kim JW, Ryu DS: Unusual bronchopulmonary foregut malformation associated with pericardial defect: bronchogenic cyst communicating with tubular esophageal duplication. J Korean Med Sci **22:**564–567, 2007
8 Heydanus R, Stewart PA, Wladimiroff JW, Los FJ: Prenatal diagnosis of congenital cystic adenomatoid lung malformation: a report of seven cases. Prenat Diagn **13:**65–71, 1993
9 Katzenstein AA, Askin FB: Surgical Pathology of Non-neoplastic Lung Disease, 2nd ed., pp. 468–506. W. B. Saunders Co., Philadelphia, PA, 1990
10 Kravitz RM: Congenital malformations of the lung. Pediatr Clin North Am **41:**453–472, 1994
11 Kwittken I, Reiner L: Congenital cystic adenomatoid malformation of the lung. Pediatrics **30:**750–768, 1962
12 Lischka A, Popow C, Horcher E, Kratochwil A, Reiner A: Problems of congenital cystic adenomatoid malformation of the lung in premature babies. Padiatr Padol **17:**465–472, 1982
13 Morelli L, Piscioli I, Licci S, Donato S, Catalucci A, Del Nonno F: Pulmonary congenital cystic adenomatoid malformation, type I, presenting as a single cyst of the middle lobe in an adult: case report. Diagn Pathol **2:**17, 2007
14 Luck SR, Reynolds M, Raffensberger JG: Congenital bronchopulmonary malformation. Curr Probl Surg **23:**245–314, 1986
15 Miller PK, Sieber WK, Yunis EJ: Congenital adenomatoid malformation of the lung. A report of 17 cases and review of the literature. Pathol Annu **15:**387–402, 1980
16 Salle B, Rebaud A, Rudigoz RC, Mellier G: Prenatal diagnosis of adenomatoid malformation of the lung. 5 cases and review of the literature. J Gynecol Obstet Biol Reprod (Paris) **22:**53–57, 1993
17 Singh M, Mitra S, Kumar L, Narang A, Rao KL, Kakkar N: Congenital cystadenomatoid malformation of lung. Indian Pediatr **37:**1269–1274, 2000
18 Stocker JT, Madewell JE, Drake RM: Congenital cystic adenomatoid malformation of the lung. Classification and morphologic spectrum. Hum Pathol **8:**155–171, 1977
19 Stocker JT, Madewell JE, Drake RM: Cystic and congenital lung disease in the newborn. Perspect Pediatr Pathol **4:**93–154, 1978

Request reprints from S. Okabayashi, The Corporation for Production and Research of Laboratory Primates, Hachimandai 1-1, Tsukuba-shi, Ibaraki 305-0843 (Japan) E-mail: okarin@primate.or.jp.

Arch Dermatol Res
DOI 10.1007/s00403-008-0873-y

ORIGINAL PAPER

Administration of Ag85B showed therapeutic effects to Th2-type cytokine-mediated acute phase atopic dermatitis by inducing regulatory T cells

Hitoshi Mori · Keiichi Yamanaka · Kazuhiro Matsuo · Ichiro Kurokawa · Yasuhiro Yasutomi · Hitoshi Mizutani

Received: 5 February 2008 / Revised: 22 May 2008 / Accepted: 20 June 2008

Abstract Increase in the number of patients with atopic dermatitis (AD) has been recently reported. T helper (Th) cells that infiltrate AD skin lesions are Th2-type dominant; reduced exposure to environmental Th1-cytokine-inducing microbes is believed to contribute to the increased number of AD patients. Regulatory type immune responses have been also associated with the occurrence of AD. It has been reported that antigen 85B (Ag85B) purified from mycobacteria is a potent inducer of Th1-type immune response in mice as well as in humans. In this study, we have examined the effect of plasmid DNA encoding Ag85B derived from *Mycobacterium kansasii* on AD skin lesions induced by oxazolone (OX) application. Th2-cytokine mediated mouse AD model with immediate type response followed by a late phase reaction was developed by repeated applications of low-dose OX to sensitized mice. Mice were immunized with plasmid DNA encoding cDNA of Ag85B before OX sensitization or during repeated elicitation phase. Both therapies were associated with significant suppression of immediate type response, clinical appearance, dermal cell infiltration, reduced IL-4 production, and augmented IFN-γ mRNA expression compared to placebo-treated mice. Additionally, increased number of Foxp3$^+$ regulatory T cells were observed in the skin sections in Ag85B treated mice. The results of this study suggest that Ag85B DNA vaccine is a potential therapy for Th2 type dermatitis.

Keywords Atopic dermatitis · Antigen 85B · Regulatory T cell

Abbreviations

AD	Atopic dermatitis
Th	T helper
BCG	*Bacillus Calmette-Güerin*
Treg	Regulatory T cell
Ag85B	Antigen 85B
OX	Oxazolone

Introduction

It is known that acute phase skin lesion in atopic dermatitis (AD) is associated with enhanced secretion of T helper (Th) 2-type cytokines [8]. Increased incidence of atopic disorders has been reported in industrialized countries; according to the hygiene hypothesis, the increase in the incidence of patients may be explained by a better lifestyle and less exposure to environmental microbes [5, 7, 28]. Environmental microbes such as mycobacteria or certain virus may promote Th1-type immune response and thus reducing atopy-associated Th2-type reaction. For instance, the study

H. Mori · K. Yamanaka · I. Kurokawa · H. Mizutani (✉)
Department of Dermatology,
Mie University Graduate School of Medicine,
2-174 Edobashi, Tsu, Mie 514-8507, Japan
e-mail: h-mizuta@clin.medic.mie-u.ac.jp

K. Matsuo
Research and Development Department,
Japan BCG Laboratory, Tokyo, Japan

Y. Yasutomi
Laboratory of Immunoregulation and Vaccine Research,
Tsukuba Primate Research Center,
National Institute of Biomedical Innovation,
Tsukuba, Ibaraki, Japan

Y. Yasutomi
Department of Immunoregulation,
Mie University Graduate School of Medicine,
Tsu, Mie, Japan

carried out in Japanese *Bacillus Calmette-Güerin* (BCG)-vaccinated school children showed that responders to tuberculin had a lower prevalence of atopic disease compared to tuberculin non-responders [28]. BCG-treated mice showed suppression of experimental allergic responses [12]. More recently, it has been shown that microbial stimulation can induce regulatory T (Treg) cells with the ability to suppress both Th1-type and Th2-type inflammation [35]. In the experimental model of pulmonary inflammation, *Mycobacterium vaccae* reduces allergic pulmonary inflammation significantly by increasing the number of Treg cells that secretes IL-10 and TGF-β[37]. These observations indicate that shift from Th2 to Th1 type immune response by mycobacteria may be used for the prevention and treatment of atopic disorders.

The specific antigens eliciting Th1-type immune responses in mycobacteria have not been elucidated so far; a recent study suggested that one of the specific proteins for Th1 development is antigen 85B (Ag85B) [31]. Ag85B is a 30-kDa major protein secreted from all *Mycobacterium* species and that belongs to the Ag85 family[4]. The Ag85B can induce a strong Th1-type immune response in mice as well as in humans [31], and DNA vaccines encoding Ag85B have been reported to protect animals from tuberculosis infection by inducing Th1 response [34, 36]. We have previously reported enhancement of anti-tumor specific CTL response using Ag85B-transfected tumor cells, and by inducing Th1-type immune responses as a vaccine adjuvant [22, 30].

The purpose of the present study was to evaluate the therapeutic efficacy of Ag85B derived from *M. kansasii* in acute phase dermatitis. Repeated applications of hapten such as oxazolone (OX) on BALB/c mice causes delayed type hypersensitivity in the beginning that changes to an immediate-type response in the late phases with elevated IgE production, and deviation of Th cell responses. The skin lesions that appear in late phases are compatible with the clinical findings as well as cytokine profile observed in AD [19, 21]. In all Ag85B-treated AD mice, the immediate type reaction is effectively suppressed and IL-4 is significantly reduced. The results of this study provide evidence for the potential usefulness of Ag85B as a novel approach for the treatment of Th2 type-mediated dermatitis such as AD.

Materials and methods

Animals

Six-week-old BALB/c male mice were purchased from Japan SLC Co. (Shizuoka, Japan) and used at the age of 7 weeks. Animal care was done according to ethical guidelines, and approved by the Institutional Board Committee for Animal Care and Use of Mie University.

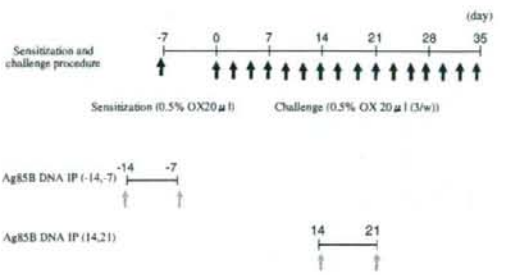

Fig. 1 Model of chronic contact hypersensitivity, and treatment with Ag85B DNA

Sensitization and challenge of animals

Oxazolone was purchased from Sigma (St Louis, MO, USA), and dissolved in acetone/olive oil (1:1). As shown in Fig. 1, mice were initially sensitized by pasting 20 μl of 0.5% OX solution to their left ear 7 days prior to the first challenge (day -7) and then 20 μl of 0.5% OX solution was repeatedly applied on the left ear three times per week from day 0. The ear swelling response was expressed as the difference between before and 30 min after application. The Ag85B expression vector pcDNA-Ag85B of *M. kansasii* open reading frame lacking a signal sequence has been constructed into KpnI–ApaI sites of pcDNA3.1 as described previously [22]. Plasmid DNAs were purified using the Plasmid Mega Kit (Qiagen, Chatsworth, CA, USA). The empty plasmid pcDNA3.1 was used as a control. Plasmid DNAs were diluted with sterilized physiological saline. Hundred micrograms per mouse of plasmid DNA was injected intraperitoneally on day -14, -7 to evaluate prophylactic effects, or on day 14 and 21 for the assessment of therapeutic effects.

Histological analysis

Skin specimens obtained 30 min after the final challenge were fixed in 10% buffered neutral formaldehyde and embedded in paraffin. Sections prepared of 7 μm thickness were stained with hematoxylin and eosin (H&E), or truidine blue.

Immunohistochemistry

The left ear was sacrificed on day 35, and was embedded in Tissue-Tek OCT compound (Miles, Elkhart, USA), frozen in liquid nitrogen, and cut with a cryostat into 7 μm-thick sections. The tissue preparations were then incubated with

primary antibodies specific for Foxp3 (eBioscience, San Diego) overnight, followed by the additional incubation with Alexa Fluor 633 conjugated secondary antibodies (Molecular Probes, Eugene, OR, USA) for 30 min at room temperature. Sections were examined under Fluoview FV1000 laser scanning confocal microscopy (Olympus, Tokyo, Japan). The numbers of $Foxp3^+$ cells were counted in high power fields; five randomly chosen fields were evaluated.

Analysis of cytokine mRNA expression in mouse ears

At 6 h after the final challenge, the left ear skin was sampled. The specimen was homogenized and mRNA was extracted using Isogen (Nippon Gene, Tokyo, Japan) according to the manufacture's instruction; 1 ml of homogenate was vigorously mixed with 200 μl of chloroform, and then centrifuged at 15,000 rpm for 15 min at 4°C. Aqueous phase was separated and mixed with 0.5 ml of 2-propanol (Nacalai Tesque, Kyoto, Japan) to precipitate RNA. After centrifugation, the precipitate was washed with 1 ml of 75% ethanol (Nacalai Tesque) and dried up. RNA was suspended in 50 μl of RNase-free water, the concentration was calculated based on the absorbance at 260 nm, and the quality was confirmed by electrophoresis. cDNA was synthesized from 10 μg of mRNA using archive kit (ABI, Foster City, CA, USA) according to the manufacturer's protocol.

Cytokine mRNA expression in skin

Real time quantitative reverse transcription-polymerase chain reaction (RT-PCR) was performed to measure transcriptional activity in the skin lesions. A 25-μl reaction mixture containing 1 μg total of cDNA, 900 nmol of each primer, and 250 nmol of TaqMan probe were mixed with 12.5 μl of TaqMan Master Mix (ABI, Foster City, CA, USA). The following primers and probes were used for the PCR reactions: mouse IL-4; forward: 5′-ACAGGAGAA GGGACGCCAT-3′, reverse: 5′-GAAGCCCTACAGAC GAGCTCA-3′, probe: 5′-TCCTCACAGCAACGAAGAA CACCACA-3′-TAMRA, IFN-γ; forward: 5′-TCAAGTG GCATAGATGTGGAAGAA-3′, reverse: 5′-TGGCTCT GCAGGATTTTCATG-3′, probe: 5′-TCACCATCCTTTT GCCAGTTCCTCCAG-3′-TAMRA, IL-10; forward: 5′-G GTTGCCAAGCCTTATCGGA-3′, reverse: 5′-ACCTGCT CCACTGCCTTGCT, probe: 5′-TGAGGCGCTGTCGTC ATCGATTTCTCCC-3′-TAMRA, TGF-β; forward: 5′-TG ACGTCACTGGAGTTGTACGG-3′, reverse: 5′-GGTTC ATGTCATGGATGGTGC-3′, probe: 5′-TTCAGCGCTC ACTGCTCTTGTGACAG-3′-TAMRA, β-actin; forward: 5′-AGAGGGAAATCGTGCGTGAC-3′, reverse: 5′-CAA TAGTGATGACCTGGCCGT-3′, probe: 5′-CACTGCCG CATCCTCTTCCTCCC-3′-TAMRA [25]. PCR was performed under the following conditions: 95°C for 10 min, then 40 cycles of 95°C for 15 s, 60°C for 1 min were carried out. Fluorescence data were collected during each annealing-extension step and analyzed by using ABI Prism SDS software version 1.9.1. All samples were normalized for to the β-actin mRNA content.

Measurement of serum IgE

Blood was collected under anesthesia 6 h after the last challenge. Serum IgE levels were determined by a sandwich enzyme-linked immunosorbent assay (BD PharMingen, CA, USA) according to the manufacturer's instructions. Optical density of each well was determined by using a microplate reader (Multiscan JX) (Thermo Electron, Yokohama, Japan). Standard curve was prepared using mouse anti-TNP IgE standard (BD PharMingen, CA, USA) diluted with PBS containing 10% FCS.

Statistical analysis

Differences in ear swelling and serum IgE levels were analyzed by the Kruskal–Wallis test. $P < 0.05$ was taken as significant.

Results

Effect of Ag85B on skin inflammation

We first examined whether Ag85B could modulate ear-swelling reaction in a mouse model of OX-induced AD like skin lesions. Repeated applications of OX cause Th2-mediated immediate type response. Ear swelling was measured with thickness gauge calipers before and 30 min after OX challenge on the pinna of the ear on day 32. In both prophylactic and therapeutic models, the administration of Ag85B significantly suppressed swelling compared to placebo-treated controls (Fig. 2a). The OX-challenged placebo-treated mice showed severe skin inflammation, however administration of Ag85B DNA reduced atopic inflammatory reactions (Fig. 2b).

Histological analysis

Histological examination in OX-challenged mice showed epidermal hyperplasia and strong intraepidermal and intradermal inflammatory cell infiltration including mononuclear cells, neutrophils, and granular cells (Fig. 3a). Both prophylactic and therapeutic administration of Ag85B DNA clearly reduced inflammatory cell infiltration and epidermal thickness. Skin sections stained with truidine blue showed decreased mast cell infiltration in Ag85B-treated mice (Fig. 3b).

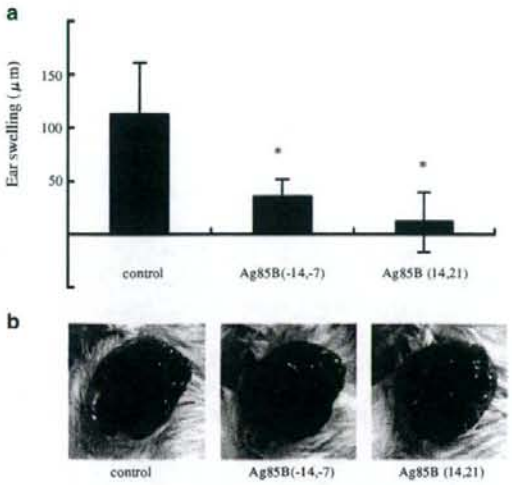

Fig. 2 **a** OX-induced ear swelling. The ear swelling response was expressed as the difference between ear thickness before and 30 min after each application on day 32. The columns and error bars represent mean ± SEM. $*P < 0.05$. Swelling was suppressed significantly in Ag85B-treated mice compared with those in placebo-treated mice. **b** Clinical features of ear skin on day 35. The OX-challenged mice showed severe skin eruption, however administration of the Ag85B DNA in both prophylactic and therapeutic models clearly reduced atopic inflammatory reactions in OX-sensitized mice

Ag85B treatment shifted the Th1/Th2 balance toward Th1

IFN-γ and IL-12 shift the Th1/Th2 balance toward Th1 condition; while IL-4 and IL-5 are key cytokines in Th2 response [24, 29]. To clarify the type of immune response in skin lesions after treatment with Ag85B, we analyzed the mRNA expression levels of IL-4 and IFN-γ by real time quantitative RT-PCR. The results were normalized to the β-actin mRNA content. As shown in Fig. 4, the expression of IL-4 mRNA was reduced in Ag85B-treated mice in both prophylactic and therapeutic models. On the contrary, the expression of IFN-γ was enhanced in Ag85B-treated mice. These results suggest that the application of Ag85B shifts the immune response toward Th1-predominace.

Total serum IgE levels

Atopic dermatitis is characterized by elevated IgE levels. Repeated applications of OX cause a gradual elevation of antigen-specific IgE level. We analyzed the degrees of IgE levels in sera collected from experimental mice. Administration of Ag85B significantly reduced the serum levels of IgE (Fig. 5).

Ag85B treatment induces regulatory T cells

TGF-β and IL-10 are important regulatory cytokines produced by Treg [11]. To investigate the mechanisms of the therapeutic effectiveness of Ag85B, we examined the mRNA levels of TGF-β and IL-10. As shown in Fig. 6a, TGF-β and IL-10 were significantly increased in Ag85B-treated mice in both prophylactic and therapeutic models. And then, we next looked at the induction of Treg in the inflamed skin. Naturally occurring $CD4^+CD25^+$ Treg are characterized by the expression of Foxp3 [10, 27]. Skin sections were stained with anti-Foxp3 mAb, and examined with a fluorescent microscope. As shown in Fig. 6b, $Foxp3^+$ cells were increased in the Ag85B-treated mice.

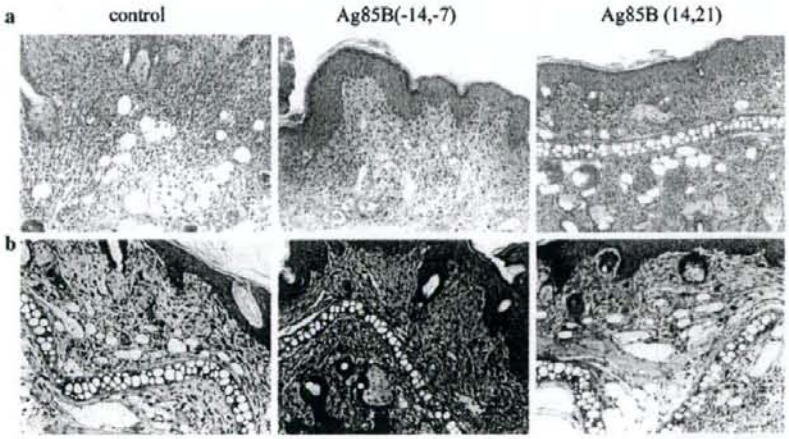

Fig. 3 Histopathological features of skin lesions. Skin was taken on day 35, paraffin embedded sections were stained with **a** hematoxylin and eosin or **b** truidine blue. OX-challenged mice showed epidermal hyperplasia along with strong intradermal inflammatory cell infiltration; whereas Ag85B DNA significantly reduced the inflammatory changes

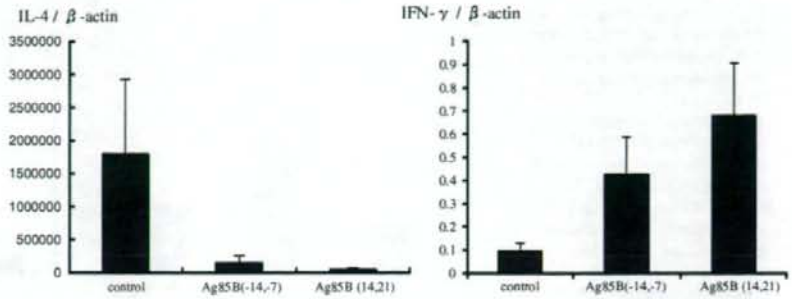

Fig. 4 mRNA expression in the ear on day 35. In order to clarify the expression of cytokine mRNA, quantitative PCR was performed by using specific primers and probes for IL-4 and IFN-γ. The expression of IL-4 mRNA was reduced in Ag85B-treated mice compared with placebo-treated mice. On the other hand, mRNA expression of IFN-γ was significantly increased in Ag85B mice

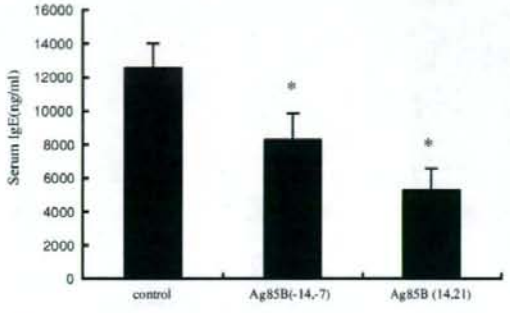

Fig. 5 Serum IgE concentrations. Serum IgE levels were measured on day 35 in control, Ag85B DNA IP (−14, −7), or Ag85B DNA IP (14, 21) mice. The columns and error bars represent mean ± SEM. $^*P < 0.05$. Administration of Ag85B reduced IgE level

Discussion

Human immune system responds to exogenous microorganisms for self-protection. These responses lead to Th1 and/ or Th2 type cytokine secretion depending on the nature of stimuli. AD is a chronic dermatitis characterized by a Th2-type immune responses that causes elevation of IgE. On the other hand, some bacterial infections including *Mycobacterium* species elicits strong Th1-type responses. Inducers of Th1 type immune response may be used as immuno-modulator having therapeutic effects against allergic disease elicited by Th2-type immune responses. Mycobacteria may affect atopic disorders by correction of the immune response from Th2 to Th1. Erb et al. reported that *M. bovis* (BCG) suppresses airway eosinophilia and associated local IL-5 production by inducing Th1-mediated response [9]. Furthermore, recent studies suggested that mycobacteria induce not only Th cells providing Th1 type immune responses but also Treg cells. In an animal model of allergy, the immunomodulatory effects of *M. vaccae* was found to be mediated by allergen-specific regulatory T lymphocytes [37], and oral administration of *M. vaccae* inhibited pulmonary allergic inflammation by induction of IL-10 [14].

Alive BCG vaccination has been used for prevention of tuberculosis. The use of *Mycobacterium* for immunomodulation requires repeated exposures to the immune system. However, repeated alive BCG vaccination is contraindicated. For human therapeutic application, it needs intradermal or intramuscular injection for vaccination. Unfortunately, cutaneous vaccination with *Mycobacterium* species commonly produces granulomatous formation leading to recalcitrant ulcers. We need to develop Th1 type immunomodulating system that induces no granulomatous reaction, if species of mycobacteria are tried to use for human. The Ag85B protein is a main component of the cell wall of mycobacteria such as *M. tuberculosis and M. kansasii* [4]; this Ag85B is known as a strong Th1 inducer in vitro [17, 18]. Experiments using plasmid DNA encoding Ag85B has been previously reported. This Ag85B is able to protect against *M. tuberculosis* even in Balb/c mice [33]. Intraperitoneal administration of Ag85B DNA inhibits granulomatous changes or adhesive reaction of intraperitoneal organs in mice (data not shown). As a preliminary study, Ag85B DNA was intradermally injected in the skin of mice skin. No ulcerative changes were observed in vaccinated areas of the skin (data not shown).

In our present study, we evaluated the efficacy of DNA encoding Ag85B for inducing Th1- and Treg-type immune response in OX-induced acute phase dermatitis. Repeated applications of OX in mice ears caused Th2-type dominant dermatitis, which mimic most of the characteristic features of AD [16, 19, 20, 32]. We first investigated whether the application of Ag85B corrects the immune response from a type Th2 one to a type Th1 response. Our results showed that Ag85B successfully ameliorates Th2-cytokine dominant immediate type reaction in the skin lesions in both prophylactic and therapeutic models of the disease. In Ag85B-treated AD skin lesion, the ear swelling was significantly reduced compared to placebo-treated animals. Administration of Ag85B DNA suppressed histological abnormalities caused by atopic inflammations such as inflammatory cell infiltration, epidermal hyperplasia, and severe edema. The presence of mast cells in the skin lesion is closely associated with Th2-type dermatitis; the number of mast cells was

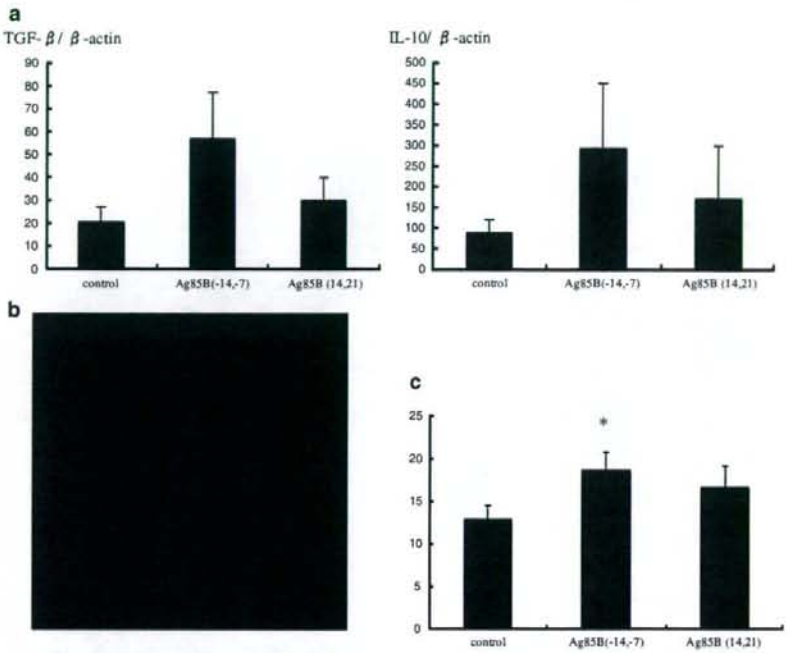

Fig. 6 **a** mRNA expression in the ear on day 35. Quantitative PCR was performed by using specific primers and probes for IL-10 and TGF-β. Both TGF-β and IL-10 were increased in the Ag85B-treated mice. **b** Foxp3$^+$ cells were clearly observed with confocal microscopy. **c** The number of Foxp3$^+$ cells per HPF was counted in five nonconsecutive fields, and Foxp3$^+$ cells were found to be increased in Ag85B-treated mice

increased in OX-treated control animals as expected; however, the number of mast cells was decreased in Ag85B-treated mice compared with controls. Enhancement of the expression of IFN-γ mRNA was significant in Ag85B-treated AD mice compared with placebo-treated animals. The expression of IL-4 mRNA were suppressed in Ag85B-treated mice compared to placebo-treated controls (Fig. 4). In addition, serum IgE levels were significantly suppressed in Ag85B treated mice compared with placebo-treated mice. These finding demonstrates that administration of Ag85B DNA significantly inhibited the development of Th2-cytokine dominant atopic inflammation by inducing Th1-type immune response.

We also examined the potential of Ag85B to induce Treg cell responses. TGF-β and IL-10 have been described as critical regulatory cytokines produced by Treg [11]. Heat-killed *M. vaccae* induces regulatory T cells that secrete IL-10 and TGF-β [37]. *M. vaccae* also induces a population of CD11$^+$ cells characterized by an increased expression of regulatory cytokines including IL-10 and TGF-β[1]. Treg cells are developed mainly in the presence of IL-10 and TGF-β [13]. More recently, Inoue and Aramaki reported that topical application of CpG-Oligodeoxynucleotides induces Foxp3$^+$ Treg in skin lesions of AD model mice in association with elevation of TGF-β[15]. Depletion of CD4$^+$CD25$^+$Treg from the peripheral blood of healthy individuals enhances proliferation of Th2 in response to various allergens [6, 23]. The mechanisms of the suppressive activity of Treg depend on cell-to-cell contact, and there is evidence for the involvement of IL-10 and TGF-β[2, 3, 26]. In this study, we have shown elevated expression of TGF-β and IL-10 in Ag85B-treated mice (Fig. 6a), and Foxp3$^+$ Treg was increased in the Ag85B-treated skin (Fig. 6b). We assume that the therapeutics capability of Ag85B is related to the induction of Foxp3$^+$Treg and Th1-type immune response.

In brief, in this study we have shown the usefulness of plasmid DNA of Ag85B for the amelioration of Th1/Th2 imbalance and for the generation of Treg cells. The observations suggest that Ag85B may be useful for the prevention and treatment of atopic disorders.

Acknowledgments This work was supported in part by Health Science Research Grants from the Ministry of Health, Labor and Welfare of Japan and the Ministry of Education, Culture, Sports, Science and Technology of Japan, Grants-in-Aid for Scientific Research and Grants-in-Aid for Core Research Evolutional Science and Technology.

Conflicts of interest statement None.

References

1. Adams VC, Hunt JR, Martinelli R, Palmer R, Rook GA, Brunet LR (2004) *Mycobacterium vaccae* induces a population of pulmonary CD11c+ cells with regulatory potential in allergic mice. Eur J Immunol 34:631–638